

The Effect of Protoplanetary Disk Cooling Times on the Formation of Gas Giant Planets by Gravitational Instability

Alan P. Boss

Department of Terrestrial Magnetism, Carnegie Institution for Science, 5241 Broad Branch Road, NW, Washington, DC 20015-1305

aboss@carnegiescience.edu

ABSTRACT

Observational evidence exists for the formation of gas giant planets on wide orbits around young stars by disk gravitational instability, but the roles of disk instability and core accretion for forming gas giants on shorter period orbits are less clear. The controversy extends to population synthesis models of exoplanet demographics and to hydrodynamical models of the fragmentation process. The latter refers largely to the handling of radiative transfer in three dimensional (3D) hydrodynamical models, which controls heating and cooling processes in gravitationally unstable disks, and hence dense clump formation. A suite of models using the β cooling approximation is presented here. The initial disks have masses of $0.091 M_{\odot}$ and extend from 4 to 20 AU around a $1 M_{\odot}$ protostar. The initial minimum Toomre Q_i values range from 1.3 to 2.7, while β ranges from 1 to 100. We show that the choice of Q_i is equal in importance to the β value assumed: high Q_i disks can be stable for small β , when the initial disk temperature is taken as a lower bound, while low Q_i disks can fragment for high β . These results imply that the evolution of disks toward low Q_i must be taken into account in assessing disk fragmentation possibilities, at least in the inner disk, i.e., inside about 20 AU. The models suggest that if low Q_i disks can form, there should be an as yet largely undetected population of gas giants orbiting G dwarfs between about 6 AU and 16 AU.

Subject headings: accretion, accretion disks – hydrodynamics – instabilities – planets and satellites: formation – protoplanetary disks

1. Introduction

Two end-member mechanisms have been proposed for gas giant planet formation, core accretion (e.g., Mizuno 1980) and gas disk gravitational instability (e.g., Cameron 1978).

The former depends on the reliable mechanism of the collisional accumulation of solid bodies, widely accepted as the formation mechanism for the terrestrial planets (e.g., Wetherill 1990, 1996). If a growing solid core should exceed a critical core mass (Mizuno 1980), its atmosphere will become unstable and the core will rapidly gain mass by accretion of gas and solids from the surrounding disk (e.g., Pollack et al. 1996), resulting in a gas giant planet. Disk instability, on the other hand, relies on the disk being massive and cold enough to become gravitationally unstable, forming spiral arms that grow and collide to form dense, self-gravitating clumps of gas and dust that might collapse and contract to form giant gaseous protoplanets (e.g., Boss 1997). Hybrid mechanisms may also be considered for forming terrestrial and gas giant planets (e.g., Boss 1998; Nayakshin 2010). Lissauer & Stevenson (2007) presented a review of the core accretion mechanism, while Durisen et al. (2007) reviewed the disk instability mechanism. More recently, Helled et al. (2014) reviewed both mechanisms, listing the strengths and weaknesses of each end-member, without reaching a definite conclusion about either mechanism. Rather, Helled et al. (2014) called for considerably more research on specific theoretical problems for both mechanisms. One problem highlighted by Helled et al. (2014) is the question about whether or not disk instability can lead successfully to giant protoplanet formation inside about 20 AU, where high optical depths in the disk mean that radiative cooling is crucial for clump formation and survival. That challenge is the focus of this paper.

We begin with a brief summary of the current status of observational constraints on giant planet formation models, both from studies of protoplanetary disks and from exoplanet detection surveys, before turning to a reconsideration of the disk radiative cooling problem that is the primary motivation for this new suite of disk instability models.

2. Observational Constraints on Theoretical Models

Observational constraints on planet formation models range from estimates of the initial conditions for planet formation, namely studies of protoplanetary disks, which provide the feedstock for planetary systems, to exoplanet demographics, the final result of the planet formation process. Disk masses, temperatures, and lifetimes are key discriminators for comparing the disk instability and core accretion mechanisms.

2.1. Protoplanetary Disk Masses

The most essential constraint is having sufficient disk mass to form a planetary system, by either core accretion or disk instability. The minimum mass solar nebula was estimated by Weidenschilling (1977) to be in the range of 0.01 to 0.07 M_{\odot} , but most citations refer only to the *minimum* of this range (0.01 M_{\odot}) as being the minimum mass solar nebula. This estimate also assumes a 100% efficient planet formation process, and so in reality these estimates of 0.01 to 0.07 M_{\odot} represent *lower bounds* on the mass of the protoplanetary disk needed to produce our solar system (Weidenschilling 1977). From this point of view, the solar nebula might well have had a mass of $\sim 0.1M_{\odot}$ or more.

Considerably more information on the range of protoplanetary disk masses is obtained by millimeter-wave astronomy. Millimeter wave observations of 11 low- and intermediate-mass pre-main-sequence stars implied that their disks formed with masses in the range from 0.05 to 0.4 M_{\odot} (Isella et al. 2009). Submillimeter wave observations of T Tauri stars in the ~ 1 Myr old Ophiuchus star-forming region imply disk masses in the range from 0.004 to 0.143 M_{\odot} (Andrews et al. 2010). Similar observations of young stars in the even younger (~ 0.5 Myr old) cluster NGC 2024 found disk masses ranging from ~ 0.003 to 0.2 M_{\odot} (Mann et al. 2015), with $\sim 10\%$ having disk masses greater than 0.1 M_{\odot} , a considerably higher fraction than in the older Taurus star-forming region. Millimeter wave observations of Class II disks in the Taurus star-forming region imply that the inferred dust disk masses scale roughly proportionally to the masses of their host stars (Andrews et al. 2013). However, estimates of total disk masses have long suffered from the uncertain conversion of the observed mass of the growing dust grains (e.g., Banzatti et al. 2011) that produce the submillimeter continuum emission to the inferred gas disk mass, potentially leading to substantial underestimates of the total disk masses (Andrews & Williams 2007). High optical depth midplanes, even at millimeter wavelengths, can lead to weak dust continuum emission and hence underestimates of the true disk mass (Forgan et al. 2016). Disk mass estimates based on observations of molecular species also depend on the assumed grain size distribution, leading to underestimated disk masses by as much as a factor of 10 (Miotello et al. 2014; Dunham et al. 2014). However, observations of the isotopologues of CO gas may offer a direct estimate of the mass of gas in protoplanetary disks (Miotello et al. 2016).

Disks with masses of $\sim 25\%$ that of their host star will be gravitationally unstable and produce spiral arms similar to those in two protoplanetary disks, MWC 758 and SAO 206462 (Dong et al. 2015). The young stellar object (YSO) Elias 2-27, with a mass of $\sim 0.5-0.6M_{\odot}$, has a protoplanetary disk with a mass of $\sim 0.04-0.14M_{\odot}$ and trailing, symmetric spiral arms that extend to the disk midplane (Pérez et al. 2016). Episodic FU Orionis outbursts in young solar-type stars are best explained by disks that are at least partially gravitationally

unstable (e.g., Zhu et al. 2007, 2009, 2010; Vorobyov & Basu 2010a,b; Liu et al. 2016). Taken together, all of these observations suggest that a significant fraction of protoplanetary disks are still gravitationally unstable during their earliest phases of evolution, when massive protostellar disks transition into less-massive protoplanetary disks.

2.2. Protoplanetary Disk Lifetimes

Disk lifetimes are another key constraint, especially for the core accretion mechanism, where gas disk lifetimes of ~ 1 Myr or longer are typically required to form gas giant planets (e.g., Pollack et al. 1996; Hubickyj et al. 2005). The conventional wisdom, based on IR excesses, is that typical disk lifetimes are in the range of 1 to 10 Myr, with an average age of ~ 3 Myr (e.g., Figure 11 in Hernandez et al. 2008). These statistics refer to young stars of different evolution classes in a variety of stellar groups. When restricting the sample to include only class III sources, Cieza et al. (2007) found that roughly $\sim 50\%$ of the youngest of 230 weak-line T Tauri stars showed no evidence for IR excesses, suggesting that half of the disks dissipate on time scales of ~ 1 Myr or less. These observations refer solely to IR excesses, wavelengths where the disks are optically thick and the dust disk mass is difficult to estimate. However, protoplanetary disks are optically thin at submillimeter wavelengths, making submillimeter dust continuum observations capable of producing more reliable dust disk masses, and hence gas disk masses. A submillimeter survey of nearly 300 YSOs in the σ Orionis cluster detected only 9 disks, finding a mean disk mass of 0.5 Jupiter masses (M_J) for these YSOs with ages of ~ 3 Myr (Williams et al. 2013), and implying that gas giant planet formation needs to finish well within 3 Myr. A similar survey of the slightly younger (2-3 Myr old) cluster IC 348 found disk masses in the range of 1.5 to 16 M_J (Cieza et al. 2015) for 13 out of the 370 cluster members, implying that disks with at least the mass ($\sim 10M_J$) of the lower bound on the minimum mass solar nebula (Weidenschilling 1977) are very rare, occurring less than about 1% of the time at the age of the IC 348 cluster. In contrast, near-IR excesses occur for roughly half of the stars in IC 348 and σ Orionis (e.g., Hernandez et al. 2008), showing that the conventional wisdom about gas disk lifetimes has been severely skewed by a reliance on IR excesses. The submillimeter surveys imply a typical gas disk lifetime closer to 1 Myr than to 3 Myr, at least for disks capable of forming gas giant planets.

2.3. Protoplanetary Disk Temperatures

Disk midplane temperatures, along with disk surface densities, determine the Toomre (1964) Q stability value, and hence the propensity for a disk to be gravitationally unstable. The solar nebula is the protoplanetary disk for which one would think we have the best information about its properties. Cometary compositions are often used to place constraints on solar nebula temperatures at their time of formation. Molecular abundance ratios determined for the comet 67P imply that if its ice grains agglomerated from clathrates (Mousis et al. 2016), then this Jupiter-family comet must have formed in a region of the solar nebula with temperatures in the range of about 32 K to 70 K (Lectez et al. 2015). Jupiter-family comets are believed to have been formed beyond Neptune, in the Kuiper Belt, whereas Oort Cloud comets are thought to have formed inward of Neptune, where Jupiter and the other giant planets could scatter them outward to much longer period orbits. Comet C/1999 S4 is a long period comet from the Oort cloud, containing ammonia ices with ortho-to-para ratios (OPR) that imply formation at a temperature of about 28 K (Kawakita et al. 2001). Measurements of the OPR for cometary water have often been used to infer even lower nebular temperatures, in the range of 10 K to 20 K (e.g., Hogerheijde et al. 2011). However, Hama et al. (2016) have disputed the commonly assumed relationship between water OPR and temperature, casting some doubt on use of the water OPR as a cometary thermometer for the solar nebula.

Other disk temperature estimates come from observations of protoplanetary disks around young solar-type stars. Observations of the DM Tau outer disk, on scales of 50 to 60 AU, imply midplane temperatures of 13 to 20 K (Dartois et al. 2003), with surface temperatures of ~ 30 K. Theoretical disk models that reproduce the observed spectral energy distributions for T Tauri-star disks typically predict disk midplane temperatures of ~ 200 K at 1 AU, ~ 40 K at 10 AU, and ~ 15 K at 100 AU (Lachaume et al. 2003; DAlessio et al. 2006). These midplane temperatures are low enough that provided the disk is massive enough, the disk is likely to be gravitationally unstable.

2.4. Exoplanets Embedded in Protoplanetary Disks

The spectacular images of the HL Tau protoplanetary disk (ALMA Partnership et al. 2015) show several gap-like structures centered on the $\sim 1.3M_{\odot}$ central protostar. HL Tau is less than 1-2 Myr old and has a disk mass of $\sim 0.03 - 0.14M_{\odot}$. Models suggest that the three main gaps at 15, 35, and 70 AU could be caused by embedded protoplanets with masses of 0.2, 0.27, and $0.55 M_J$ (Dipierro et al. 2015). A direct imaging search for embedded planets in the 70 AU gap placed only upper limits of $\sim 10 - 15M_J$ on the unseen objects (Testi et

al. 2015). Testi et al. (2015) noted that Boss (2011) showed that the HL Tau disk could form a $\sim 5M_J$ planet at 70 AU by disk instability, a planet massive enough to cause the gap, but not massive enough to have been directly imaged. Akiyama et al. (2016) have shown that all of the observed gaps in the HL Tau disk are consistent with gas giant formation by disk instability, coupled with inward migration. Embedded planets can also generate spiral arms in marginally gravitationally unstable disks (Pohl et al. 2015). Carrasco-Gonzalez et al. (2016) have used the VLA to study the HL Tau disk, finding that the inner disk has fragmented and formed dense clumps, suggesting gravitational instability as the cause (see also Mayer et al. 2016). The HL Tau system thus may represent the foremost poster child for gas giant planet formation by disk gravitational instability.

The HL Tau disk is threaded with a magnetic field that is coincident with its major axis (Stephens et al. 2014), implying that the field does not control the dynamics of the disk. In a related vein, recent work on the Allende meteorite has shown that its magnetization was derived from its parent body, not the solar nebula (Fu et al. 2014), implying that the dynamics of the midplane of the solar nebula were not dominated by magnetic forces. Hence non-magnetic disk instability models appear to be relevant to both the HL Tau disk and the solar nebula, and presumably to other protoplanetary disks as well.

2.5. Exoplanet Demographics

The ultimate constraints on theoretical models of planetary formation are derived from the results of the ongoing world-wide effort to determine the population statistics of exoplanets with widely varying masses, mean densities, atmospheric compositions, and orbital properties. The spectacular discoveries of thousands of exoplanets by the Kepler Mission (Borucki et al. 2010, 2011a,b) have revolutionized the field, and made possible direct comparisons with the predictions of exoplanet population synthesis (EPopS) models based on the core accretion mechanism. Perhaps most dramatically, the Kepler detections imply that the number of planets per star appears to be a roughly monotonically increasing function of decreasing exoplanet radius (Fressin et al. 2013), at least down to radii of $\sim 2R_\oplus$ (Earth radii), contrary to the predictions of EPopS models. Early EPopS models (e.g., Ida & Lin 2005, 2008) were based on the population uncovered primarily by radial velocity (RV) and ground-based transit photometry surveys and were able to select model parameters that fit reasonably well the exoplanets known at the time. These models (e.g., Figure 3 in Ida & Lin 2008) predicted a dearth of planets with masses in the super-Earth mass range and short period orbits (i.e., inside ~ 1 AU), the so-called *exoplanet desert* (Ida & Lin 2004), as well as a surplus of hot Jupiters and hot super-Earths orbiting at ~ 0.03 AU. On the contrary,

Kepler found an *exoplanet oasis* where the EPopS predicted a desert: Batalha (2014) showed that Kepler had found the highest frequency of exoplanets in the region where the desert had been predicted, and no evidence for a pile-up of hot exoplanets with orbital periods of a few days. The same problem besets the more recent EPopS models of Alibert et al. (2011) and Mordasini et al. (2012). EPopS models with a new prescription for orbital migration have filled in part of the desert, but only at the cost of over-producing massive gas giants and shifting the desert upward to higher masses (see Figure 8 in Dittkrist et al. 2014; see also Coleman & Nelson 2014). Evidently EPopS models based solely on core accretion are not yet able to find a combination of parameters that enables them to reproduce the Kepler findings. EPopS models that include gas giant planet formation by disk instability (e.g., Forgan & Rice 2013) might offer a means to escape some of the inward orbital migration and surplus gas giant planet problems that beset pure core accretion EPopS models by shortening gas disk lifetimes, and by stopping cores from migrating inward and growing to become gas giants.

The Kepler Mission’s 4-yr survey of the field in Cygnus-Lyra prohibited the detection of exoplanets with orbital periods greater than about 1 yr. Other techniques shed light on the demographics at greater distances. E.g., an RV survey of 202 solar-type stars that had been followed for 17 yrs found a frequency of $\sim 6\%$ for giant planets orbiting from 3 to 7 AU (Wittenmyer et al. 2016). The combination of Adaptive Optics (AO) imaging and a long-term RV survey found a total occurrence rate of $52 \pm 5\%$ for exoplanet masses in the range of 1-20 M_J at distances of 5 to 20 AU (Bryan et al. 2016), with a suggestion that most have orbital distance less than 10 AU. This fraction is higher than that found earlier by Cumming et al. (2008), who found that 8 yrs of RV data implied that up to 20% of stars have gas giants within 20 AU. Evidently longer survey periods find increasing frequencies of long-period exoplanets, as expected. Hence even the current estimates should be considered lower bounds.

Microlensing surveys also sample a different portion of exoplanet discovery space compared to transit photometry surveys like Kepler, namely orbital distances comparable to the Einstein radius, which means orbital distances of a few AU and orbital periods of a few years for solar-type stars. Cassan et al. (2012) found their microlensing data to reveal that $\sim 17\%$ of stars host planets with masses in the range of 0.3 to 10 M_J , while lower mass planets are even more common. With more recent data, Shvartzvald et al. (2016) found that $\sim 55\%$ of these low mass (K-M dwarf) stars hosted planets, with Neptune-mass planets being about 10 times as common as Jupiter-mass planets. Sumi et al. (2011) interpreted short-time-scale microlensing events (less than 2 days) as evidence for a population of unbound or distant Jupiter-mass objects that are about twice as common as main-sequence stars. Sumi et al. (2011) argued that these objects were most likely to be unbound gas giants that were ejected

from protoplanetary disks, but Veras & Raymond (2012) found that planet-planet scattering could not be expected to form that many objects. Their analysis was restricted to gas giants formed by core accretion, i.e., their planets were initially located at a few AU from their stars. Ma et al. (2016) similarly found that core accretion could not produce the number of ejected planets implied by the Sumi et al. (2011) observations. Forgan et al. (2015) and Vorobyov (2016), on the other hand, propose that disk fragmentation in the outer disk regions will lead to the frequent ejection of brown dwarfs and gas giants, perhaps explaining the Sumi et al. (2011) results. Even if these objects are bound, their orbits must lie beyond 10 AU from their stars, a region where disk instability is likely to be the main formation mechanism, rather than core accretion (see below). Contrary to the assertions by Sumi et al. (2011), direct imaging surveys searching for such distant but bound gas giants do not exclude the microlensing population from being bound objects (Quanz et al. 2012). Either way, gravitational instability seems to be implicated in explaining the Sumi et al. (2011) gas giant population.

2.6. Directly Imaged Exoplanets on Wide Orbits

The discovery of the HR8799 bcde exoplanet system (Marois et al. 2008, 2010) is as remarkable in its own way as the millimeter-wave image of the HL Tau disk (ALMA Partnership et al. 2015). This system consists of *four* gas giant planets with masses of about 5 to 7 M_J , orbiting at distances of about 14, 24, 38, and 68 AU from an A5 star of 1.5 M_\odot with an age of ~ 30 Myr. 51 Eridani is a younger (~ 20 Myr) F0IV star with a mass of $1.75 \pm 0.05 M_\odot$ and with a $\sim 2M_J$ planet orbiting at a distance of ~ 13 AU (Macintosh et al. 2015). HD 100546 is an even younger (~ 10 Myr) Herbig Ae/Be star with a mass of $2.4 \pm 0.1 M_\odot$, which has a gas giant planet orbiting at a distance of ~ 53 AU, and a possible second planet at ~ 14 AU (Quanz et al. 2015). Finally, LkCa 15 is an extremely young (~ 2 Myr) solar-type star with two likely protoplanets orbiting ~ 15 and 19 AU away, with planet masses no greater than $\sim 5 - 10M_J$ being required for orbital stability (Sallum et al. 2015).

The M0 close binary system ROXs 42B is orbited at ~ 150 AU by a third body with a mass in the range of 6 to 15 M_J (Currie et al. 2014). This third object appears to blur the line between exoplanets (with masses less than $\sim 13M_J$), such as the HR 8799 bcde planetary system (Marois et al. 2008; 2010), and brown dwarfs. It also therefore blurs the line between the formation mechanisms of wide and close binary stars, brown dwarfs, and possibly of gas giant exoplanets, namely protostellar and protoplanetary disk fragmentation (Currie et al. 2014). As one example, Konopacky et al. (2016) found a brown dwarf companion with a

mass of $\sim 30M_J$ orbiting 20 AU from HR 2562, a $1.3 M_\odot$ star with a debris disk. Such brown dwarfs are widely believed to form by disk fragmentation, based on both observational (e.g., Ma & Ge 2014) and theoretical (e.g., Li et al. 2015) evidence.

2.7. Giant Planet Formation on Wide Orbits

Given the observational evidence for a growing number of extrasolar giant planets orbiting at distances well beyond the orbits of Jupiter and Saturn, the question arises as to their formation mechanism. The formation of the solar system’s outer giant planets, Uranus and Neptune, is considered problematical for the core accretion (CA) mechanism. Levison et al. (2015) claimed to have solved the problem of forming all four of the solar system’s giant planets by relying on the pebble accretion mechanism (e.g., Bitsch et al. 2015) to grow giant planet cores rapidly, before the solar nebula gas disappeared. Their CA models led to the formation of 1 to 4 giant planets between 5 and 15 AU, as desired. However, their initial conditions consisted of a protoplanetary disk that is assumed to be passive, with a surface density profile (Figure 1) that is nearly identical to that of the gravitationally unstable disk models studied by Boss (2013, 2015) and by this paper. Such a moderately massive disk will not be passive, however, and the resulting spiral arms will play havoc with the orbits of the solid bodies that are trying to grow by pebble accretion, as shown by Boss (2013, 2015). As a result, the formation of even the solar system’s outer giant planets should be considered to remain problematical. Bromley & Kenyon (2016) studied CA models in disks as massive as $0.5 M_\odot$ in order to try to explain the possible existence of a massive, ninth planet orbiting beyond 100 AU, yet another challenge for solar system formation models.

Chambers (2006) studied the CA process in a disk with a radius of 50 AU, and found that no giant planets more massive than $\sim 0.2M_J$ were formed beyond ~ 8 AU. Kenyon & Bromley (2015) found that in a suitably massive disk, CA could lead to the formation of an icy super-Earth at distances of 125 to 250 AU, but that this would require 1 to 3 Gyr, roughly a factor of 10^3 times too slow to allow such an icy core to accrete a gaseous envelope and form a gas giant. Chambers (2016) studied CA in the pebble accretion scenario for disks with radii of 50 to 100 AU, finding that gas giant planet formation was limited to orbital distances of ~ 15 AU or less. A similar result was found in the CA models of Coleman & Nelson (2016). At best, CA would seem to require the formation of massive icy cores in the inner disk, which are then scattered to the outer disk by close encounters with one or more inner gas giants. Once in the outer disk, the icy cores could accrete outer disk gas, which could circularize their initially highly eccentric orbits (Kikuchi et al. 2014). However, objects formed by this mechanism are predicted to be extremely rare, occurring in only \sim

0.1% of the cases studied by population synthesis models (Kikuchi et al. 2014). Such a scattering process is also likely to be hazardous to the health of inner terrestrial planets (Kaib & Chambers 2016).

On the other hand, Boss (2011) found that disk instability (DI) could form numerous gas giants with initial masses in the range of 1 to 5 M_J , initial distances of 30 to 70 AU, and initial eccentricities of ~ 0 to 0.35, around solar-type protostars with masses from 0.1 to 2 M_\odot . The initial disk mass was assumed to scale with the protostellar mass, with the result that the more massive stars had more giant exoplanets, as expected. Forming the HR 8799 exoplanet system thus seems quite possible through the DI mechanism (Boss 2011). In fact, forming gas giants at large distances by disk instability has now become a part of the conventional wisdom of planet formation theory (e.g., Boley 2009; Boley & Durisen 2010; Boley et al. 2010; Nero & Bjorkman 2009; Meru & Bate 2010; Kratter & Murray-Clay 2011; Rogers & Wadsley 2012; Vorobyov et al. 2013; Madhusudhan et al. 2014; Rice et al. 2015; Young & Clarke 2016). Meru (2015) found that fragments formed by DI in the outer disk could even trigger the formation of more fragments in the inner disk.

Galvagni et al. (2012) found that clumps formed by DI in the outer disk at ~ 100 AU could contract fast enough ($\sim 10^3$ yr) to begin rapid dynamic collapse without being tidally disrupted. Nayakshin (2015a,b) showed that pebble accretion by a gaseous protoplanet could accelerate its collapse by changing its opacity, again helping avoid tidal disruption. Boss (2013) found that giant planets orbiting in a marginally gravitationally unstable disk did not undergo monotonic orbital migration, but rather underwent random inward and outward excursions, driven by the gravitational actions of the spiral arms, for several thousand years or more. Stamatellos (2015) found that a giant planet formed in the outer disk would soon open a disk gap, preventing its migration to the inner disk (cf., Vorobyov 2013), and that it would not accrete sufficient gas to become a brown dwarf, rather than a gas giant planet (cf., Kratter et al. 2010).

3. Hydrodynamical Models of Disk Instability

Given this strong observational evidence that a mechanism similar to disk instability must be able to form at least some exoplanets, it behooves us to consider the current status of disk instability theoretical modeling efforts. We first note the present status of the more computationally challenging models that involve 3D radiative transfer, and then introduce the computationally simpler β cooling approach.

3.1. Radiative Transfer Models

Boss (1997) began the detailed study of DI with 3D models that used simplified thermodynamics for the gaseous disk, namely isothermal or adiabatic gas pressure laws. Boss (2001) then calculated the first DI models with 3D radiative transfer (i.e., radiation hydrodynamics - RHD), finding that disk fragmentation was still possible. Boley et al. (2006) found in their 3D RHD models that the clumps that formed did not last long. Durisen et al. (2007) summarized much of the detailed work on 3D radiative transfer models of the DI mechanism, both from the side of models where clump formation occurred (e.g., Boss 2001, 2002, 2007; Mayer et al. 2007) and from models where clump formation was less robust (e.g., Boley et al. 2006, 2007). While many numerical factors come to play in these calculations, e.g., grid resolutions for finite difference (FD) codes and smoothing lengths for smoothed-particle hydrodynamics (SPH) codes (e.g., Mayer et al. 2007), flux limiters for radiative transfer in the diffusion approximation, and accuracy of the gravitational potential solver, the key issue was determined to be whether a protoplanetary disk could remain sufficiently cold for spiral arms to collide and form self-gravitating clumps that could contract toward planetary densities without re-expanding, being disrupted by tidal forces from the central protostar, or meeting some other equally unkind fate, i.e., the radiative transfer solver. Boley et al. (2006) showed that their cylindrical coordinate RHD code could reproduce an analytical radiative transfer solution, while Boss (2009) demonstrated the agreement of his spherical coordinate RHD code on two other analytical radiative transfer solutions. Helled et al. (2014) updated the situation in their review paper without reaching a definitive conclusion regarding the validity of the DI hypothesis in RHD models (e.g., the work by Boss 2008, 2009, 2010, 2011, 2012; Boley & Durisen 2008, 2010; Boley 2009; Cai et al. 2010; Meru & Bate 2010). More recently, Steiman-Cameron et al. (2013) studied the effect of spatial resolution on cooling times in RHD models, finding convergence for optically thick, inner regions, but not for optically thin, outer regions. Tsukamoto et al. (2015) used 3D RHD models to follow the formation of disks, starting from collapsing molecular cloud cores, finding that radiative heating from the interstellar medium could have a significant effect on the fragmentation process.

3.2. Beta Cooling Models

Gammie (2001) suggested that the outcome of gravitational instability depended on the beta parameter $\beta = t_{cool}\Omega$, where t_{cool} is the disk cooling time and Ω is the local angular velocity. Gammie (2001) found that for $\beta > 3$, the disk would become gravitoturbulent with a Toomre Q value ~ 1 , whereas for $\beta < 3$, the disk would fragment. Lodato & Rice (2004) and Mejia et al. (2005) also discussed the importance of cooling times for disk fragmentation.

The use of the critical value of $\beta = 3$ to predict the fragmentation of protoplanetary disks was first called into question by the 3D SPH hydrodynamical models of Meru & Bate (2011a,b), who found that when sufficiently high spatial resolution was employed, even disks previously thought to be stable underwent fragmentation into clumps. Meru & Bate (2011b) even suggested that in the absence of clear indications of numerical convergence, a critical value might not exist. Meru & Bate (2012) found evidence for convergence with both 3D SPH and 2D FD (FARGO) codes on a critical value of $\beta > 20$, and perhaps as large as ~ 30 .

Gammie (2001) had studied two dimensional (2D), shearing-sheet disk models with a maximum numerical resolution of 1024^2 . Baehr & Klahr (2015) also studied 2D shearing sheet models, but with a refined cooling law, and found that with their highest resolution models (4096^2), the 2D disks fragmented even for $\beta = 10$, but not when the resolution was 2048^2 with $\beta = 10$. Paardekooper (2012) studied 2D shearing sheet models with the FARGO FD code, finding fragmentation to occur for β values as high as 20, provided the integration was followed long enough in time.

Rice et al. (2014), however, argued that numerical problems involving the implementation of the disk cooling in SPH codes and the handling of artificial viscosity in both SPH and the FARGO FD codes may have led to higher critical β values. They claimed that their SPH simulations converged on a critical value of β between 6 and 8. However, Zhu et al. (2015) have shown that SPH models will not converge to the continuum limit if only the total number of particles (N) is increased to ∞ ; formal numerical convergence is only possible when $N \rightarrow \infty$, the smoothing length $h \rightarrow 0$, and the number of neighbor particles within the smoothing volume $N_{nb} \rightarrow \infty$. The latter constraint is seldom applied, lending suspicion to the claims of numerical convergence of many previous SPH studies.

Young & Clarke (2015) used both 2D SPH and 2D finite difference models to suggest two possible pathways to fragmentation: dynamic collapse when $\beta < 3$, or quasi-static contraction when $\beta < 12$, for models with effectively 2048^2 resolutions. Evidently even for simplified β cooling prescriptions, enough numerical questions and differences remain that the critical β value for fragmentation, if there is one, cannot be constrained better than to lying in the range of ~ 10 to ~ 30 .

3.3. Initial Toomre Q Values

Takahashi et al. (2016) pointed out the crucial importance of the Toomre Q value: fragmentation occurs when the Toomre Q value drops to ~ 0.6 inside the spiral arms, regardless of the value of β , and that low β values do not necessarily result in fragmentation.

Gammie (2001) studied 2D disks with $Q = 1$ initially. The Paardekooper (2012) and Baehr & Klahr (2015) 2D models also started with $Q = 1$ throughout the disk. Young & Clarke (2015) started with disks with $Q \approx 1$. Meru & Bate (2012) and Rice et al. (2014) started with disks with a minimum of $Q = 2$ at the outer disk edge. Rafikov (2015) has argued that gravitoturbulent disks without rapid cooling should settle into a quasi-stationary, fluctuating state where Q remains close to a constant value $Q_0 \sim 1$. The concept of a quasi-steady balance of disk heating and cooling dates back to Pringle (1981), and has been investigated in many models by the Indiana University group (e.g., Steiman-Cameron et al. 2013), yielding $Q \sim 1.5$ to 2. This balance has been suggested to be an alternative to fragmentation (e.g., Durisen et al. 2007).

Backus & Quinn (2016) found that the critical initial value of Q for fragmentation depended on how stable the initial disk equilibrium model was: less stable initial disk equilibria fragmented for higher Q values. Evidently initial Q values in the range of 1 to 2 are considered reasonable starting values for DI models with β cooling.

4. Numerical Methods

In order to allow a direct comparison with previous work, the new models were calculated with the same basic code that has been used in all of the author’s previous studies of disk instability. The primary change was to replace the radiative transfer subroutine that calculates the energy changes due to radiative flux with the β cooling formula. The numerical code solves the three dimensional equations of hydrodynamics and the Poisson equation for the gravitational potential and is second-order-accurate in both space and time. A complete description of the entire code is given by Boss & Myhill (1992), while the updated energy equation of state is described by Boss (2007). Also, the central protostar is effectively forced to wobble in order to preserve the location of the center of mass of the entire system (Boss 1998, 2012), which is accomplished by altering the apparent location of the point mass source of the star’s gravitational potential in order to balance the center of mass of the disk. Central massive sink cell particles behave in exactly this same way to preserve the center of mass of the system when used in, for example, the FLASH hydrodynamics code.

As usual, explicit artificial viscosity (AV) is not used in the models. Boss (2006) found that small amounts of tensor AV had little effect on fragmentation, while large amounts could suppress fragmentation, as was also found by Pickett et al. (2000). AV is designed to stabilize and capture the microphysics of heating in strong shocks, and the effect of its inclusion in β cooling models remains to be investigated.

The numerical code solves the specific internal energy E equation (Boss & Myhill 1992):

$$\frac{\partial(\rho E)}{\partial t} + \nabla \cdot (\rho E \mathbf{v}) = -p \nabla \cdot \mathbf{v} + L,$$

where ρ is the gas density, t is time, \mathbf{v} is the velocity, p is the gas pressure, and L is the time rate of change of energy per unit volume, which is normally taken to be that due to the transfer of energy by radiation in the diffusion approximation. Here we define L in terms of the β cooling formula (Gammie 2001), as follows. With $\beta = t_{cool}\Omega$, t_{cool} is defined as the ratio of the specific internal energy to the time rate of change of the specific internal energy. We thus define L to be:

$$L = -\frac{\rho E \Omega}{\beta},$$

where Ω is the local angular velocity of the gas in prograde rotation ($\Omega > 0$). Evidently L is always negative with this formulation, i.e., only cooling is permitted.

It is important to note that in spite of the β cooling formula, the disk temperature at a given radial distance from the central protostar is not allowed to fall below its initial value. This means that initially high Q disks cannot become more gravitationally unstable solely due to cooling to lower temperatures than the initial state, regardless of the cooling parameter β , and can only become gravitationally unstable by transporting disk mass such that the local disk surface density increases, thereby lowering Q locally. This assumption is critical to understanding the results to be presented for initially high Q disk models. This minimum temperature constraint was also imposed in all of the previous disk instability models in this series, and so was retained here in order to allow a direct comparison with those earlier models. A future paper will address the outcome of models similar to these, but where the disk temperature is allowed to cool below the initial value. An alternative justification for this temperature constraint is to consider the case of disks being heated by protostellar irradiation, e.g., Cai et al. (2008) and Takahashi et al. (2016), in which case disks might become hot enough to suppress fragmentation altogether.

The equations are solved on a spherical coordinate grid with $N_r = 100$ or 200 radial grid points (as well as the central grid cell, which contains the central protostar), $N_\theta = 23$ theta grid points, distributed from $\pi/2 \geq \theta \geq 0$, and $N_\phi = 512$ or 1024 azimuthal grid points. N_r and N_ϕ are increased to their higher values once the disk forms dense spiral arms and the Jeans and Toomre length criteria begin to be violated (see below). The radial grid is uniformly spaced with either $\Delta r = 0.16$ AU or 0.08 AU, for $N_r = 101$ or 200, respectively. The radial grid extends from 4 to 20 AU. The mass of disk gas flowing inside 4 AU is

added to the central protostar, whereas that reaching the outermost shell at 20 AU loses its outward radial momentum but remains on the active hydrodynamical grid. The θ grid points are compressed into the midplane to ensure adequate vertical resolution ($\Delta\theta = 0.3^\circ$ at the midplane). The ϕ grid is uniformly spaced in 2π . The number of terms in the spherical harmonic expansion for the gravitational potential of the disk is $N_{Y_{lm}} = 48$ for all phases of evolution.

The numerical resolution is increased during the evolutions in order to avoid violating the Jeans length (e.g., Boss et al. 2000) and Toomre length criteria (Nelson 2006). Both criteria are monitored throughout the evolutions (e.g., Boss 2011) to ensure that any clumps that might form are not numerical artifacts. The Jeans length criterion consists of requiring that all of the grid spacings in the spherical coordinate grid remain smaller than 1/4 of the Jeans length $\lambda_J = \sqrt{\frac{\pi c_s^2}{G\rho}}$, where c_s is the local sound speed, and G the gravitational constant. Similarly, the Toomre length criterion consists of requiring that all of the grid spacings remain smaller than 1/4 of the Toomre length $\lambda_T = (2c_s^2/G\Sigma)$, where Σ is the mass surface density. When one of these two criteria is violated, the calculation is halted, and the grid spatial resolution is doubled in either the radial or azimuthal direction, as necessary, by dividing each cell into half in the relevant direction. Mass and momentum are conserved by this process.

Once well-defined clumps form, the Jeans and Toomre length criteria will eventually again be violated at the maximum densities of the clumps, even with the $N_r = 200$ and $N_\phi = 1024$ grids. At this point, the cell with the maximum clump density is drained of 90% of its mass and momentum, which is then used to form a virtual protoplanet (VP) initially at the cell center (e.g., Boss 2005, 2013). The VPs thereafter orbit around the disk, subject to the gravitational forces of the disk gas and the central protostar, as well as those of any other VPs. The disk gas is similarly subject to the gravity of the VPs. VPs that orbit to the inner boundary at 4 AU or to the outer boundary at 20 AU are simply removed from the remainder of the evolutions. The VPs are allowed to gain mass \dot{M} at the rate (Boss 2005, 2013) given by the Bondi-Hoyle-Lyttleton (BHL) formula (e.g., Ruffert & Arnett 1994):

$$\dot{M} = \frac{f4\pi\rho(GM)^2}{(v^2 + c_s^2)^{3/2}},$$

where f is a dimensionless coefficient, M is the VP mass, and v is the speed of the VP respect to the disk gas. The VPs also accrete orbital angular momentum from the disk gas, by accreting an amount of momentum from the local hydrodynamical cell proportional to the mass being accreted from that cell in such a way as to guarantee the conservation of the total orbital angular momentum. This insertion of VPs in regions where the Jeans and

Toomre length criteria can no longer be met is identical to the manner in which *sink particles* are inserted into adaptive mesh refinement codes, such as FLASH, when no further sub grids are allowed to be formed (e.g., Federrath et al. 2010; Klassen et al. 2014).

These models used $f = 1$ in order to maximize the gas accretion by the VPs and to minimize subsequent Jeans or Toomre length violations. If the Jeans or Toomre criterion is nevertheless subsequently violated in the immediate vicinity (10 cells) of an existing VP, the violation is ignored, as the VP is expected to accrete or disrupt this high density gas. Violations more than 10 cells away result in the creation of a new VP. Along with the maximum spatial resolution required, the number of VPs formed thus gives a basic estimate of the extent to which a given set of initial conditions leads to a gravitationally unstable disk capable of fragmenting into clumps.

5. Initial Conditions

The models all begin from the same initial disk model as that used by Boss (2001, 2005, 2007, 2008, 2012, 2013), differing only in the minimum initial Toomre Q value and the β parameter. The initial density is that of an adiabatic, self-gravitating, thick disk in near-Keplerian rotation about a stellar mass M_s (Boss 1993):

$$\rho(R, Z)^{\gamma-1} = \rho_o(R)^{\gamma-1} - \left(\frac{\gamma-1}{\gamma}\right) \left[\left(\frac{2\pi G\sigma(R)}{K}\right)Z + \frac{GM_s}{K} \left(\frac{1}{R} - \frac{1}{(R^2 + Z^2)^{1/2}}\right) \right],$$

where R and Z are cylindrical coordinates, $\sigma(R)$ is the surface density, $K = 1.7 \times 10^{17}$ (cgs units) and $\gamma = 5/3$. The initial midplane density ensures near-Keplerian rotation throughout the disk:

$$\rho_o(R) = \rho_{o4} \left(\frac{R_4}{R}\right)^{3/2},$$

where $\rho_{o4} = 10^{-10}$ g cm⁻³ and $R_4 = 4$ AU, the inner edge of the numerical grid. The resulting initial disk mass is $0.091 M_\odot$, while the initial protostellar mass is $M_s = 1.0 M_\odot$. Note that this initial approximate equilibrium disk state does not depend explicitly on the outer disk temperature, and was chosen to be a state dominated by rotational support rather than by gas pressure, at least in the radial direction (Boss 1993). As a result, this same initial density distribution is used for all the models, regardless of the variations in the outer disk temperatures.

Table 1 lists the initial conditions chosen for the models. The initial outer disk temperatures T_o are varied in order to alter the initial minimum values of the Toomre (1964) Q gravitational stability parameter, decreasing monotonically outward from highly stable $Q_{max} = 9$ values at 4 AU to marginally stable Q_{min} values ranging from 1.3 to 2.7 beyond 10 AU. Values of β of 1, 3, 10, 20, 30, 40, 50, and 100 were used in the models. These choices for the initial disk conditions, Q_{min} , and β are consistent with the observational constraints and with the papers on β cooling models that were cited previously.

Figure 1 shows the initial surface density profile for the models, compared to the power law assumed in the core accretion models by Levison et al. (2015). We shall see that the passive disk assumed in these core accretion models is likely to be gravitationally unstable for realistic disk midplane temperatures. Figure 2 displays the initial Toomre (1964) Q profiles for three representative sets of models, those with outer disk temperatures of 40 K, 90 K, and 180 K, leading to initial minimum Q values beyond 10 AU of 1.3, 2.0, and 2.7, respectively. Midplane temperatures at the inner disk edge at 4 AU are 600 K for all models, while the outer disk temperatures are varied as listed in Table 1. The initial midplane temperature profiles are based on the 2D RHD models by Boss (1996), as used by Boss (2001, 2005, 2007, 2008, 2012).

Figure 3 displays the initial midplane density distribution for all of the models, along with the initial midplane temperature distribution for the models with initial minimum Toomre $Q_i = 1.3$, i.e., the models with outer disk temperatures of 40 K. While the initial temperature distributions are perfectly axisymmetric about the rotation axis (center of each plot), the initial density distributions are non-axisymmetric at a low level: random cell-to-cell noise at the level of 1% has been added to the density distribution, along with $m = 1, 2, 3$, and 4 modes of amplitude 0.01, as in previous models (e.g., Boss 1998).

6. Results

Table 1 lists the basic results for all of the models, namely the final times reached, the final spatial resolution employed, and the maximum number of virtual planets (N_{VP}) that formed and existed simultaneously, usually close to the final number of VPs. The final times reached ranged from 244 yrs to 978 yrs. For comparison, the initial orbital period of the disk at the inner edge (4 AU) was 8.0 yr, whereas the initial orbital period at the outer edge (20 AU) was 91 yrs. The key point is that all the models were evolved far enough in time that there was no evidence for any further significant growth of non-axisymmetry, i.e., no need to further refine the spatial grid. Some models still required the creation of additional VPs, but this was balanced by the loss of VPs that hit either the inner or outer grid boundaries,

indicating that a semblance of a steady state configuration had been reached. Because the Boss & Myhill (1992) code employed has not been parallelized, each model was computed continuously on a single, dedicated cluster core. Most models were run for as long as 2.3 yrs on the DTM flash cluster, while others were run for as long as 7 months on the considerably faster Carnegie memex cluster at Stanford University.

Figure 4 summarizes the results from Table 1 as follows. Models where the initial spatial resolution of $N_r = 100$ and $N_\phi = 512$ sufficed for the entire evolution without violating the Jeans or Toomre constraints experienced little growth of non-axisymmetry (red dots), while those that needed to be refined to $N_r = 200$ with $N_\phi = 512$ experienced moderate growth (green dots), and those that ended with $N_r = 200$ and $N_\phi = 1024$ experienced significant growth of spiral arms (blue dots). The remaining models continued to violate the Jeans or Toomre criteria, even with $N_r = 200$ and $N_\phi = 1024$, necessitating the creations of VPs at the location of the violations. The black symbols in Figure 4 represent the maximum number of VPs created for those models, ranging from a black circle for a single VP, to a bar for two VPs, to a three-pointed star for three VPs, etc.

Figure 4 demonstrates that the assumed initial conditions are just as important for determining the success of a possible disk gravitational instability in forming self-gravitating clumps as is the choice of the β cooling parameter. All of the models with $Q_i = 1.3$ fragmented and formed from 4 to 10 VPs, regardless of the cooling rates investigated, from $\beta = 1$ to $\beta = 100$. This somewhat surprising result means that if a disk is initially extremely gravitationally unstable, self-gravitating clumps can form rapidly without being stifled by compressional heating during their assembly. However, the time at which the first VP formed depended strongly on the value of β , with the first VP in models 1.3-1 and 1.3-3 forming after 104 yrs and 118 yrs, respectively, compared to forming only after 190 yrs and 212 yrs, respectively, for models 1.3-50 and 1.3-100. Clearly even for an initially highly unstable disk, the cooling rate affects the time evolution of the fragmentation process. At the same time, the models starting with $Q_i = 2.7$ show that such an initially gravitationally stable disk cannot become non-axisymmetric enough to undergo fragmentation, even for $\beta = 1$. As noted previously, this result is largely a result of the constraint that the disk temperatures cannot drop below their initial values, in spite of vigorous cooling, and can only become more gravitationally unstable by increasing the disk surface density in a limited region of the disk, e.g., by forming a ring. For initial Toomre Q values in between these two extremes, the general result is a smooth progression toward more of a tendency toward fragmentation at a fixed value of β (e.g., for $\beta = 3$ and 10 as Q_i is lowered). However, the transition from stable to unstable with regard to forming VPs is not necessarily completely monotonically dependent on Q_i (i.e., for $\beta = 1$ and 100, where as Q_i is decreased, successive models can fragment and then resist fragmentation, before eventually fragmenting again). This result

demonstrates the stochastic nature of gravitationally unstable disks, where the spiral arms that form repeatedly and interact with each other may or may not happen to combine in a constructive wave sense and form a clump dense enough to require the creation of a VP. Given this ambiguity, the critical value for fragmentation appears to be $\beta_c \sim 1$ for $Q_i \sim 2.2$, $\beta_c \sim 10$ for $Q_i \sim 1.9$, and $\beta_c \sim 50$ for $Q_i \sim 1.6$, roughly speaking.

Figure 5 presents the final midplane density distributions for the four models at the extremes of the parameter space investigated, namely models 1.3-1, 1.3-100, 2.7-1, and 2.7-100. The two models with $Q_i = 1.3$ both clearly formed numerous spiral arms and clumps, regardless of whether $\beta = 1$ or 100, though in the latter case the spiral arms are broader and nowhere near as sharply defined. Neither of the two models with $Q_i = 2.7$ formed any significant non-axisymmetric features, and the model with $\beta = 100$ looks the most similar to the initial disk model (Figure 3a), in spite of having evolved for 414 yrs. Figure 6 displays the corresponding midplane temperature distributions for these same four end-member models. The slower cooling rate in model 1.3-100 (Figure 6b) compared to that of 1.3-1 results in well-defined, moderately warm spiral arms throughout the disk, whereas the rapid cooling assumed in model 1.3-1 (Figure 6a) allows the disk to cool back down to its initial temperature throughout most of the disk. For the high Q_i models, Figure 6c shows that model 2.7-1 maintains a disk temperature essentially unchanged from its initial conditions, as a result of the rapid cooling, whereas in Figure 6d, model 2.7-100 shows several distinct rings of somewhat hotter gas than the initial temperature distribution.

Figure 7 shows the location of the nine VPs still active in model 1.3-1 at the end of the evolution (224 yrs), the same time as the midplane density contours shown in Figure 5a. It is evident that the nine VPs are not aligned with the numerous spiral arm features seen in Figure 5a, as is to be expected, given that the VPs begin their existence with an initial mass of the order of a fraction of a Jupiter mass, and as such are not subject to the tendency for gas drag to force small (e.g., cm-size) particles to remain in the vicinity of spiral arms (e.g., Boss 2013, 2015).

The time evolution of the ensemble of VPs formed in the eight models with $Q_i = 1.3$ is presented in Figure 8, sampled roughly every 40,000 time steps. Starting with masses only a small fraction of a Jupiter mass, the VPs accrete mass at the BLH rate and soon reach masses as high as $5 M_J$. The VPs tend to be created in the sweet spot between 6 AU and 10 AU, where the disk is cool enough and massive enough to support the growth of strong spiral arms. Once formed there, the VPs can migrate through disk interactions (e.g., Boss 2013) both inwards and outwards, with significant numbers hitting either the inner or outer disk boundaries and thereafter being removed from the calculations.

Finally, Figure 9 compares the VPs formed in the $Q_i = 1.3$ models with the presently

known distribution in mass and semi-major axis of exoplanets between 4 AU and 20 AU. While not intended to be a rigorous exoplanet population synthesis on a par with those presented in Section 2.5, Figure 9 hints that the disk instability mechanism may be able to crudely match the exoplanet demographics for gas giants with semi-major axes of 4 AU to 6 AU, and if so, this approach would predict an as yet mostly undetected significant population of Jupiter-mass gas giants orbiting at distances of about 6 AU to 16 AU. Refining the implications of these disk instability models for explaining the known exoplanet demographics, and for predicting what more might be discovered by future exoplanet surveys (e.g., by microlensing and direct imaging searches with the NASA WFIRST mission) is a promising subject for further work.

7. Discussion

These models were intended in part to provide a comparison between the disk stability models previously presented in this series (e.g., Boss 2001, 2007, 2008, 2012), which employed diffusion approximation radiative transfer, with new models using the β cooling approach. The previous models all explored variations on numerical parameters such as spatial grid resolution, equations of state, temperature assumptions, and diffusion approximation flux-limiters, with the result that the disks, with initial $Q_{min} = 1.3$, nevertheless fragmented into clumps. Given the results found here for the $Q_{min} = 1.3$ initial disks, which all formed numerous VPs, even with β as high as 100, the basic results of the previous diffusion approximation models starting from these initial conditions do not appear to be as contentious as they have at times seemed (e.g., Durisen et al. 2007; Helled et al. 2014).

Section 2.3 noted that several indicators of protoplanetary disk temperatures at distances of ~ 10 to 20 AU imply midplane temperatures of ~ 40 to 70 K, i.e., values of Q_i from about 1.3 to 1.7 for the present disk models. Figure 4 shows that such disks are unstable to fragmentation on short time scales, regardless of the assumed value of β . Figure 1 shows that these disk models have an initial surface density profile quite similar to that assumed in the Levison et al. (2015) models of solar system formation by pebble accretion. Evidently the background passive gas disk adopted for the Levison et al. (2015) efforts is unlikely to be passive, calling into question their results regarding the formation of our giant planets.

Boss (2004) found evidence in 3D diffusion approximation models of disk instability for convective upwellings that were able to cool the outer disk at a rate equivalent to $\beta \sim 6$, leading to fragmentation, as expected based on the results shown in Figure 4 [Note, however, that Boley & Durisen (2006) and Lyra et al. (2016) have interpreted such upwellings as hydraulic jumps, rather than as the result of convection.] As previously noted, Meru & Bate

(2011b) suggested that a critical value of β for fragmentation might not exist, a suspicion that is supported by the weak dependence of the results shown in Figure 4 on β for a fixed value of Q_i , i.e., the initial conditions assumed are more important in general than the choice of β . Takahashi et al. (2016) found a similar result to that seen in Figure 4, namely that fragmentation can occur whenever Q becomes sufficiently small, regardless of β , and that low β alone does not guarantee fragmentation. In particular, Takahashi et al. (2016) found that fragmentation would occur when Q dropped to 0.6 in a spiral arm. Figure 10 displays the radial profile of Q in model 1.3-1 at the time (104 yrs) when a VP needed to be inserted into the calculation: it can be seen that the minimum azimuthally averaged value of Q at that time was 0.61, seemingly in remarkable agreement with the results of Takahashi et al. (2016). However, for the seven other models with $Q_i = 1.3$, the equivalent minimum Q value ranges from 0.69 to 1.0. Given that these are azimuthally averaged Q values, however, the basic agreement with Takahashi et al. (2016) holds. In fact, the first VP in model 1.3-1 was inserted at 7.2 AU, the radius of the innermost local minimum in the azimuthally averaged Q seen in Figure 10. The Q value of the actual midplane grid cell where this first VP was inserted was ~ 0.1 , considerably lower still.

8. Conclusions

The present set of models has shown that the disk instability mechanism for gas giant planet formation depends even more strongly on the initial conditions assumed in the models than on the assumed disk cooling rate β , based on a suite of 3D models with identical handling of the spatial resolution of the grid. Hence the evolution of protoplanetary disks into gravitationally unstable configurations is as important a factor to consider as the detailed heating and cooling processes in the disks. The models imply that if a significant fraction of protoplanetary disks can form that are similar to those assumed here, then there should be an equally significant population of gas giants remaining to be discovered with separations of order 15 AU from solar-type stars. The NASA WFIRST mission may very well test this prediction, based on a combination of exoplanet searches by gravitational microlensing and by coronagraphic direct imaging.

In order to help determine what is the proper value of β to use in disk instability models, the author is currently running a suite of eight flux-limited diffusion approximation (FLDA) models similar to the present suite, with initial minimum Q values ranging from 1.3 to 2.7, and with the same approach of adding spatial resolution and VPs when demanded by the Jeans and Toomre criteria, with the goal of comparing these results for varied beta cooling models with those of FLDA models, for the same spatial resolution and same initial

conditions (i.e., initial Toomre Q). Previous FLDA disk instability models by Boss (2008, 2012) used different spatial resolutions than the present models and so cannot be used for a valid comparison. However, the suite of models currently running will allow the proper value of β that should be used in disk instability models to be determined, as opposed to determining the critical value of β for fragmentation for a given initial disk model, which was the goal of the present work.

In order to better understand the approach to gravitational instability, a second set of eight models with the β cooling approximation is also currently underway. These models all start from the same $Q_{min} = 2.7$ model as in this paper, and with same range of eight β values as here, but with the minimum disk temperature values all relaxed to 40 K (i.e., relaxed to the outer disk minimum temperature for the highly unstable models with initial $Q_{min} = 1.3$). These models will thus study the effect of varied cooling rates on the approach to a gravitationally unstable phase of disk evolution.

I thank the referee, Richard Durisen, for a number of perceptive and constructive comments on the manuscript, and Sandy Keiser for computer systems support. The calculations were performed primarily on the flash cluster at DTM and also on the Carnegie memex cluster at Stanford University.

REFERENCES

- Adams, F. C., Ruden, S. P., & Shu, F. H. 1989, *ApJ*, 347, 959
- Akiyama, E., Hasegawa Y., Hayashi, M., & Iguchi, S. 2016, *ApJ*, 818, 158
- ALMA Partnership et al. 2015, *ApJL*, 808, L3
- Alibert, Y., Mordasini, C., & Benz, W. 2011, *A&A*, 526, A63
- Andrews, S. M., & Williams, J. P. 2007, *ApJ*, 659, 705
- Andrews, S. M., Rosenfeld, K. A., Kraus, A. L., & Wilner, D. J. 2013, *ApJ*, 771, 129
- Andrews, S. M., Wilner, D. J., Hughes, A. M., Qi, C., & Dullemond, C. P. 2010, *ApJ*, 723, 1241
- Backus, I., & Quinn, T. 2016, *MNRAS*, 463, 2480
- Baehr, H., & Klahr, H. 2015, *ApJ*, 814, 155
- Banzatti, A., Testi, L., Isella, A., Natta, A., Neri, R., & Wilner, D. J. 2011, *A&A*, 525, A12
- Batalha, N. 2014, *PNAS*, 111, 12647
- Bitsch, B., Lambrechts, M., & Johansen, A. 2015, *A&A*, 582, A112

- Boley, A. C. 2009, *ApJ*, 695, L53
- Boley, A. C., & Durisen, R. H. 2006, *ApJ*, 641, 534
- Boley, A. C., & Durisen, R. H. 2008, *ApJ*, 685, 1193
- Boley, A. C., & Durisen, R. H. 2010, *ApJ*, 724, 618
- Boley, A. C., Durisen, R. H., Nordlund, A., & Lord, J. 2007, *ApJ*, 665, 1254
- Boley, A. C., Hayfield, T., Mayer, L., & Durisen, R. H. 2010, *Icarus*, 207, 509
- Boley, A. C., Mejía, A. C., Durisen, R. H., Cai, K., Pickett, M. K., & D’Alessio, P. 2006, *ApJ*, 651, 517
- Borucki, W., et al. 2010, *Science*, 327, 977
- Borucki, W., et al. 2011a, *ApJ*, 728, 117
- Borucki, W., et al. 2011b, *ApJ*, 736, 19
- Boss, A. P. 1993, *ApJ*, 417, 351
- Boss, A. P. 1996, *ApJ*, 469, 906
- Boss, A. P. 1997, *Science*, 276, 1836
- Boss, A. P. 1998, *ApJ*, 503, 923
- Boss, A. P. 2001, *ApJ*, 563, 367
- Boss, A. P. 2002, *ApJ*, 567, L149
- Boss, A. P. 2004, *ApJ*, 610, 456
- Boss, A. P. 2005, *ApJ*, 629, 535
- Boss, A. P. 2006, *ApJ*, 641, 1148
- Boss, A. P. 2007, *ApJ*, 661, L73
- Boss, A. P. 2008, *ApJ*, 677, 607
- Boss, A. P. 2009, *ApJ*, 694, 107
- Boss, A. P. 2010, *ApJ*, 725, L145
- Boss, A. P. 2011 *ApJ*, 731, 74
- Boss, A. P. 2012, *MNRAS*, 419, 1930
- Boss, A. P. 2013, *ApJ*, 764, 194
- Boss, A. P. 2015, *ApJ*, 807, 10
- Boss, A. P., & Myhill, E. A. 1992, *ApJS*, 83, 311

- Boss, A. P., Fisher, R. T., Klein, R. I., & McKee, C. F. 2000, *ApJ*, 528, 325
- Bromley, B. C., & Kenyon, S. J. 2016, *ApJ*, 826, 64
- Bryan, M. L., et al. 2016, *ApJ*, 821, 89
- Cai, K., Durisen, R. H., Boley, A. C., Pickett, M. K., & Mejia, A. C. 2008, *ApJ*, 673, 1138
- Cai, K., Pickett, M. K., Durisen, R. H., & Milne, A. M. 2010, *ApJ*, 716, L176
- Cameron, A. G. W. 1978, *Moon Planets*, 18, 5
- Carrasco-Gonzalez, C., et al. 2016, *ApJL*, 821, L16
- Cassan, A., et al. 2012, *Nature*, 481, 167
- Chambers, J. E. 2006, *ApJL*, 652, L133
- Chambers, J. E. 2016, *ApJ*, 825, 63
- Cieza, L., et al. 2007, *ApJ*, 667, 308
- Cieza, L., et al. 2015, *MNRAS*, 454, 1909
- Coleman, G. A. L., & Nelson, R. P. 2014, *MNRAS*, 445, 479
- Coleman, G. A. L., & Nelson, R. P. 2016, *MNRAS*, 460, 2779
- Cumming, A., et al. 2008, *PASP*, 120, 531
- Currie, T., et al. 2014, *ApJL*, 780, L30
- DAlessio, P., Calvet, N., Hartmann, L., Franco-Hernandez, R., & Servin, H. 2006, *ApJ*, 638, 314
- Dartois, E., Dutrey, A., & Guilloteau, S. 2003, *A&A*, 399, 773
- Dipierro, G., Price, D., Laibe, G., Hirsh, K., Cerioli, A., & Lodato, G. 2015, *MNRAS*, 453, L73
- Dittkrist, K.-M., Mordasini, C., Klahr, H., Alibert, Y., & Henning, T. 2014, *A&A*, 567, A121
- Dong, R., Hall, C., Rice, K., & Chiang, E. 2015, *ApJL*, 812, L32
- Dunham, M. M., Vorobyov, E. I., & Arce, H. G. 2014, *MNRAS*, 444, 887
- Durisen, R. H., Boss, A. P., Mayer, L., Nelson, A., Rice, K., & Quinn, T. R. 2007, in *Protostars and Planets V*, B. Reipurth, D. Jewitt, & K. Keil, eds. (Tucson: University of Arizona Press), 607
- Federrath, C., Banerjee, R., Clark, P. C., & Klessen, R. S. 2010, *ApJ*, 713, 269
- Forgan, D., Parker, R. J., & Rice, K. 2015, *MNRAS*, 447, 836
- Forgan, D., & Rice, K. 2013, *MNRAS*, 423, 3168

- Forgan, D. H., Ilee, J. D., Cyganowski, C. J., Brogan, C. L., & Hunter, T. R. 2016, *MNRAS*, 463, 957
- Fressin, F., et al. 2013, *ApJ*, 766, 81
- Fu, R. R., Lima, E. A., & Weiss, B. P. 2014, *EPSL*, 404, 54
- Galvagni, M., Hayfield, T., Boley, A., Mayer, L., Roskar, R., & Saha, P. 2012, *MNRAS*, 427, 1725
- Gammie, C. F. 2001, *ApJ*, 553, 174
- Hama, T., Kouchi, A., & Watanabe, N. 2016, *Science*, 351, 65
- Helled, R., et al. 2014, in *Protostars and Planets VI*, H. Beuther et al., eds. (Tucson: University of Arizona Press), 643
- Hernandez, J., et al. 2008, *ApJ*, 686, 1195
- Hogerheijde, M. R., et al. 2011, *Science*, 334, 338
- Hubickyj, O., Bodenheimer, P., & Lissauer, J. J. 2005, *Icarus*, 179, 415
- Ida, S., & Lin, D. N. C. 2004, *ApJ*, 604, 388
- Ida, S., & Lin, D. N. C. 2005, *ApJ*, 626, 1045
- Ida, S., & Lin, D. N. C. 2008, *ApJ*, 685, 584
- Isella, A., Carpenter, J. M., & Sargent, A. I. 2009, *ApJ*, 701, 260
- Kaib, N., & Chambers, J. E. 2016, *MNRAS*, 455, 3561
- Kawakita, H., et al. 2001, *Science*, 294, 1089
- Kenyon, S. J., & Bromley, B. C. 2015, *ApJ*, 806, 42
- Kikuchi, A., Higuchi, A., & Ida, S. 2014, *ApJ*, 797, 1
- Klassen, M., et al. 2014, 797, 4
- Konopacky, Q. M., et al. 2016, *ApJL*, 829, L4
- Kratter, K. M., Murray-Clay, R. A., & Youdin, A. N. 2010, *ApJ*, 710, 1375
- Lachaume, R., Malbet, F., & Monin, J.-L. 2003, *A&A*, 400, 185
- Lectez, S., et al. 2015, *ApJL*, 805, L1
- Levison, H. F., Kretke, K. A., & Duncan, M. J. 2015, *Nature*, 524, 322
- Li, Y., Kouwenhoven, M. B., Stamatellos, D., & Goodwin, S. P. 2015, *MNRAS* 805, 116
- Lissauer, J. J., & Stevenson, D. J. 2007, in *Protostars and Planets V*, B. Reipurth, D. Jewitt, & K. Keil, eds. (Tucson: University of Arizona Press), 591

- Liu, H. B., et al. 2016, *Science Advances*, Vol. 2, No. 2, id.e1500875
- Lodato, G., & Rice, W. K. M. 2004, *MNRAS*, 351, 630
- Lyra, W., et al. 2016, *ApJ*, 817, 102
- Ma, B., & Ge, J. 2014, *MNRAS*, 439, 2781
- Ma, S., Mao, S., Ida, S., Zhu, W., & Lin, D. N. C. 2016, *MNRAS*, 461, L107
- Macintosh, B., et al. 2015, *Science*, 350, 64
- Madhusudhan, N., Amin, M. A., & Kennedy, G. M. 2014, *ApJL*, 794, L12
- Mann, R. K., et al. 2015, *ApJ*, 802, 77
- Marois, C., Macintosh, B., Barman, T., Zuckerman, B., Song, I., Patience, J., Lafrenière, D., & Doyon, R. 2008, *Science*, 322, 1348
- Marois, C., Zuckerman, B., Konopacky, Q. M., Macintosh, B., & Barman, T. 2010, *Nature*, 468, 1080
- Mayer, L., Lufkin, G., Quinn, T., & Wadsley, J. 2007, *ApJ*, 661, L77
- Mayer, L., Peters, T., Pineda, J. E., Wadsley, J., & Rogers, P. 2016, *ApJL*, 823, L36
- Mejia, A. C., Durisen, R. H., Pickett, M. K., & Cai, K. 2005, *ApJ*, 619, 1098
- Meru, F. 2015, *MNRAS*, 454, 2529
- Meru, F., & Bate, M. R. 2010, *MNRAS*, 409?, 858
- Meru, F., & Bate, M. R. 2011a, *MNRAS*, 410, 559
- Meru, F., & Bate, M. R. 2011b, *MNRAS*, 411, L1
- Meru, F., & Bate, M. R. 2012, *MNRAS*, 427, 2022
- Miotello, A., Bruderer, S., & van Dishoeck, E. F. 2014, *A&A*, 572, A96
- Miotello, A., van Dishoeck, E. F., Kama, M., & Bruderer, S. 2016, *A&A*, 594, A85
- Mizuno, H. 1980, *Prog. Theor. Phys.*, 64, 544
- Mordasini, C., Alibert, Y., Klahr, H., & Henning, T. 2012, *A&A*, 547, A111
- Mousis, O., et al. 2016, *ApJL*, 819, L33
- Nayakshin, S. 2010, *MNRAS*, 408, L36
- Nayakshin, S. 2015a, *MNRAS*, 446, 459
- Nayakshin, S. 2015b, *MNRAS*, 448, L25
- Nelson, A. F. 2006, *MNRAS*, 373, 1039
- Nero, D., & Bjorkman, J. E. 2009, *ApJ*, 702, L163

- Paardekooper, S.-J. 2012, MNRAS, 421, 3286
- Pérez, L. M., et al. 2016, Science, 353, 1519
- Pickett, B. K., et al. 2000, ApJ, 529,1034
- Pohl, A., et al. 2015, MNRAS, 453, 1768
- Pollack, J. B., Hubickyj, O., Bodenheimer, P., Lissauer, J. J., Podolak, M., & Greenzweig, Y. 1996, Icarus, 124, 62
- Pringle, J. E. 1981, ARAA, 19, 137
- Quanz, S. P., Lafreniere, D., Meyer, M. R., Reggiani, M. M., & Buenzli, E. 2012, A&A, 541, A133
- Quanz, S. P., Amara, A., Meyer, M. R., Girard, J. H., Kenworthy, M. A., & Kasper, M. 2015, ApJ, 807, 64
- Rafikov, R. R. 2015, ApJ, 804, 62
- Rice, K., Lopez, E., Forgan, D., & Biller, B. 2015, MNRAS, 454, 1940
- Rice, W. K. M., Paardekooper, S.-J., Forgan, D. H., & Armitrage, P. J. 2014, MNRAS, 438, 1593
- Rogers, P. D., & Wadsley, J. 2012, MNRAS, 423, 1896
- Ruffert, M., & Arnett, D. 1994, ApJ, 427, 351
- Sallum, S., et al. 2015, Nature, 527, 342
- Shvartzvald, Y., et al. 2016, MNRAS, 457, 4089
- Stamatellos, D. 2015, ApJL, 810, L11
- Steiman-Cameron, T., Durisen, R. H., Boley, A. C., Michael, S., & McConnell, C. R. 2013, ApJ, 768
- Stephens, I. W., et al. 2014, Nature, 514, 597
- Sumi, T., et al. 2011, Nature, 473, 349
- Takahashi, S. Z., Tsukamoto, Y., & Inutsuka, S. 2016, MNRAS, 458, 3597
- Testi, L, et al. 2015, ApJL, 812,L38
- Toomre, A. 1964, ApJ, 139, 1217
- Tsukamoto, Y., Takahashi, S. Z., Machida, M. N., & Inutsuka, S. 2015, MNRAS, 446, 1175
- Veras, D., & Raymond, S. N. 2012, MNRAS, 421, L117
- Vorobyov, E. I. 2013, A&A, 552, A129

- Vorobyov, E. I. 2016, *A&A*, 590, A115
- Vorobyov, E. I., & Basu, S. 2010a, *ApJL*, 714, L133
- Vorobyov, E. I., & Basu, S. 2010b, *ApJ*, 719, 1896
- Weidenschilling, S. J. 1977, *ApSS*, 51, 153
- Wetherill, G. W. 1990, *AREPS*, 18, 205
- Wetherill, G. W. 1996, *Icarus*, 119, 219
- Williams, J. P., et al. 2013, *MNRAS*, 435, 1671
- Wittenmyer, R. A., et al. 2016, *ApJ*, 819, 28
- Young, M. D., & Clarke, C. J. 2015, *MNRAS*, 451, 3987
- Young, M. D., & Clarke, C. J. 2016, *MNRAS*, 455, 1438
- Zhu, Q., Hernquist, L., & Li, Y. 2015, *ApJ*, 800, 6
- Zhu, Z., et al. 2007, *ApJ*, 669, 483
- Zhu, Z., Hartmann, L., Gammie, C., & McKinney, J. C. 2009, *ApJ*, 701, 620
- Zhu, Z., Hartmann, L., & Gammie, C. 2010, *ApJ*, 713, 1143

Table 1. Initial conditions and results for the models.

Model	T_o (K)	Q_i	β	final time (yrs)	final N_r	final N_ϕ	maximum N_{VP}
1.3-1	40	1.3	1	244.	200	1024	10
1.3-3	40	1.3	3	291.	200	1024	5
1.3-10	40	1.3	10	275.	200	1024	6
1.3-20	40	1.3	20	378.	200	1024	5
1.3-30	40	1.3	30	302.	200	1024	5
1.3-40	40	1.3	40	285.	200	1024	4
1.3-50	40	1.3	50	306.	200	1024	9
1.3-100	40	1.3	100	342.	200	1024	5
1.6-1	60	1.6	1	312.	200	1024	3
1.6-3	60	1.6	3	270.	200	1024	6
1.6-10	60	1.6	10	263.	200	1024	2
1.6-20	60	1.6	20	319.	200	1024	2
1.6-30	60	1.6	30	263.	200	1024	1
1.6-40	60	1.6	40	293.	200	1024	2
1.6-50	60	1.6	50	295.	200	1024	3
1.6-100	60	1.6	100	799.	200	512	0
1.7-1	70	1.7	1	358.	200	1024	1
1.7-3	70	1.7	3	327.	200	1024	3
1.7-10	70	1.7	10	292.	200	1024	4
1.7-100	70	1.7	100	393.	200	1024	3
1.9-1	80	1.9	1	394.	200	1024	5
1.9-3	80	1.9	3	286.	200	1024	3
1.9-10	80	1.9	10	413.	200	1024	1
1.9-100	80	1.9	100	470.	200	1024	1
2.0-1	90	2.0	1	235.	200	1024	3
2.0-3	90	2.0	3	383.	200	1024	3
2.0-10	90	2.0	10	351.	200	1024	1
2.0-100	90	2.0	100	315.	200	1024	0
2.1-1	100	2.1	1	354.	200	512	0
2.1-3	100	2.1	3	486.	200	1024	0
2.1-10	100	2.1	10	896.	200	1024	0

Table 1—Continued

Model	T_o (K)	Q_i	β	final time (yrs)	final N_r	final N_ϕ	maximum N_{VP}
2.1-100	100	2.1	100	490.	200	512	0
2.2-1	120	2.2	1	415.	200	1024	1
2.2-3	120	2.2	3	697.	200	512	0
2.2-10	120	2.2	10	772.	100	512	0
2.2-100	120	2.2	100	978.	100	512	0
2.7-1	180	2.7	1	450.	100	512	0
2.7-3	180	2.7	3	454.	100	512	0
2.7-10	180	2.7	10	414.	100	512	0
2.7-100	180	2.7	100	414.	100	512	0

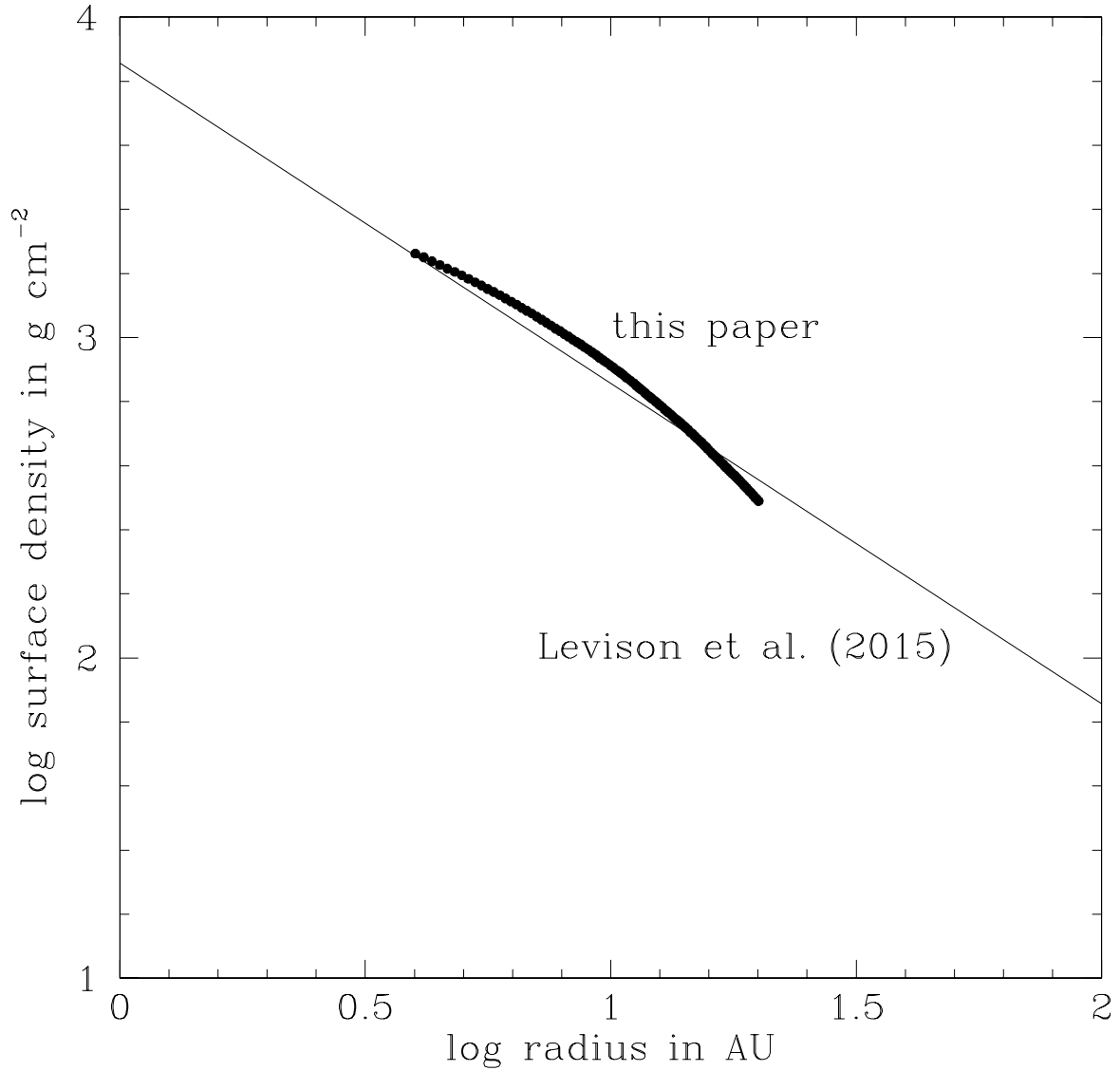


Fig. 1.— Initial disk surface density profile for all the models, compared to that assumed in the core accretion models by Levison et al. (2015). The present model disks all have an inner radius of 4 AU and an outer radius of 20 AU, for a total disk mass of $0.091 M_{\odot}$.

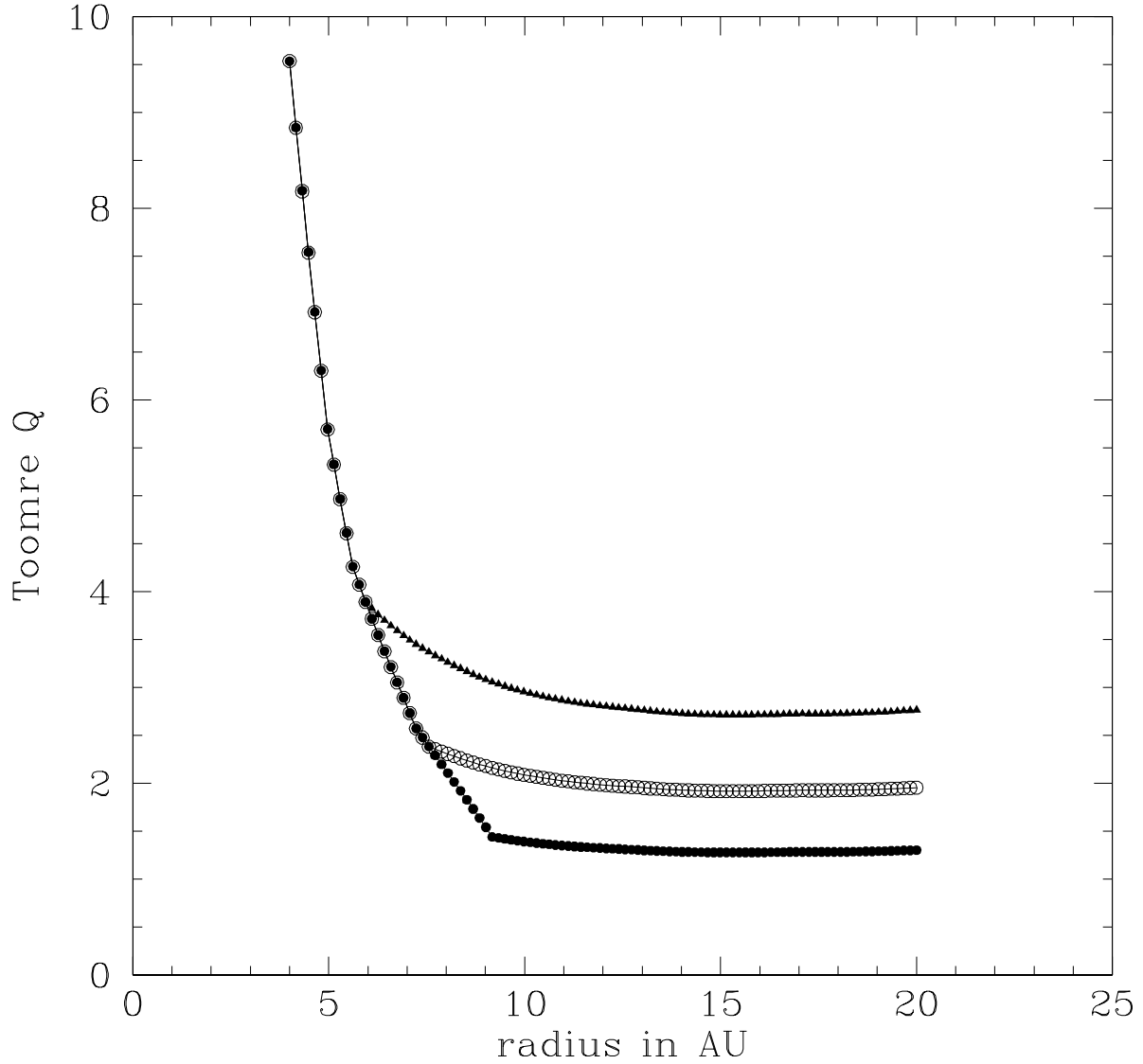


Fig. 2.— Initial Toomre (1964) Q stability parameter as a function of disk radius for models with outer disk temperatures of 40 K, 90 K, and 180 K, leading to initial minimum Q values (Q_i) beyond 10 AU of 1.3 (bottom), 2.0 (middle), and 2.7 (top), respectively.

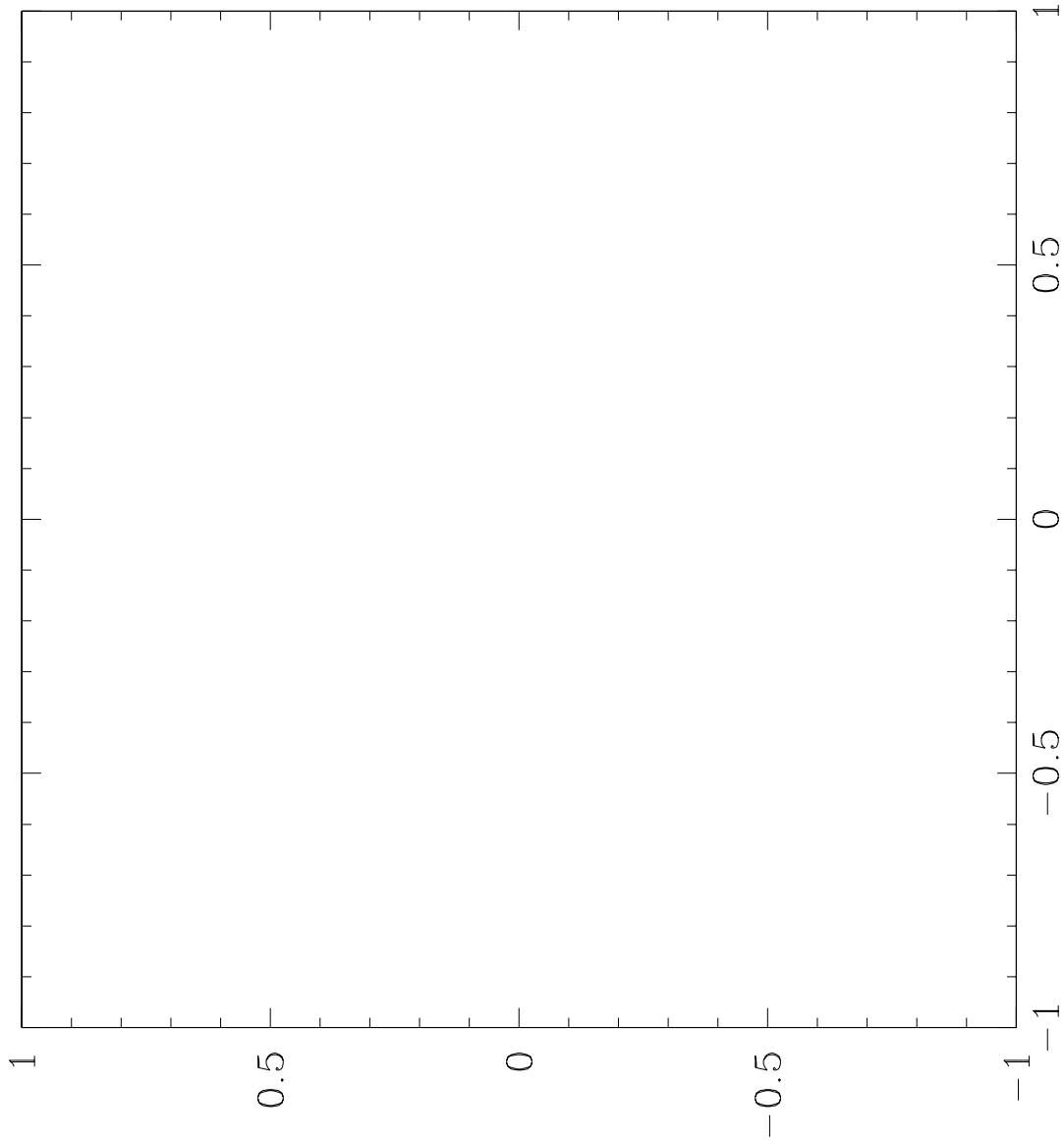


Fig. 3.— Note: Inclusion of Figure 3 violates the file size limits for arxiv. You may download the entire pdf file from this web page: <https://home.dtm.ciw.edu/users/boss/ftp/beta-cooling.pdf>. Caption for Figure 3: Equatorial (midplane) density (a) and temperature (b) contours for model 1.3-1 at the beginning of the evolution. The disk has an inner radius of 4 AU and an outer radius of 20 AU. Contours are labelled in log cgs and log K units, respectively.

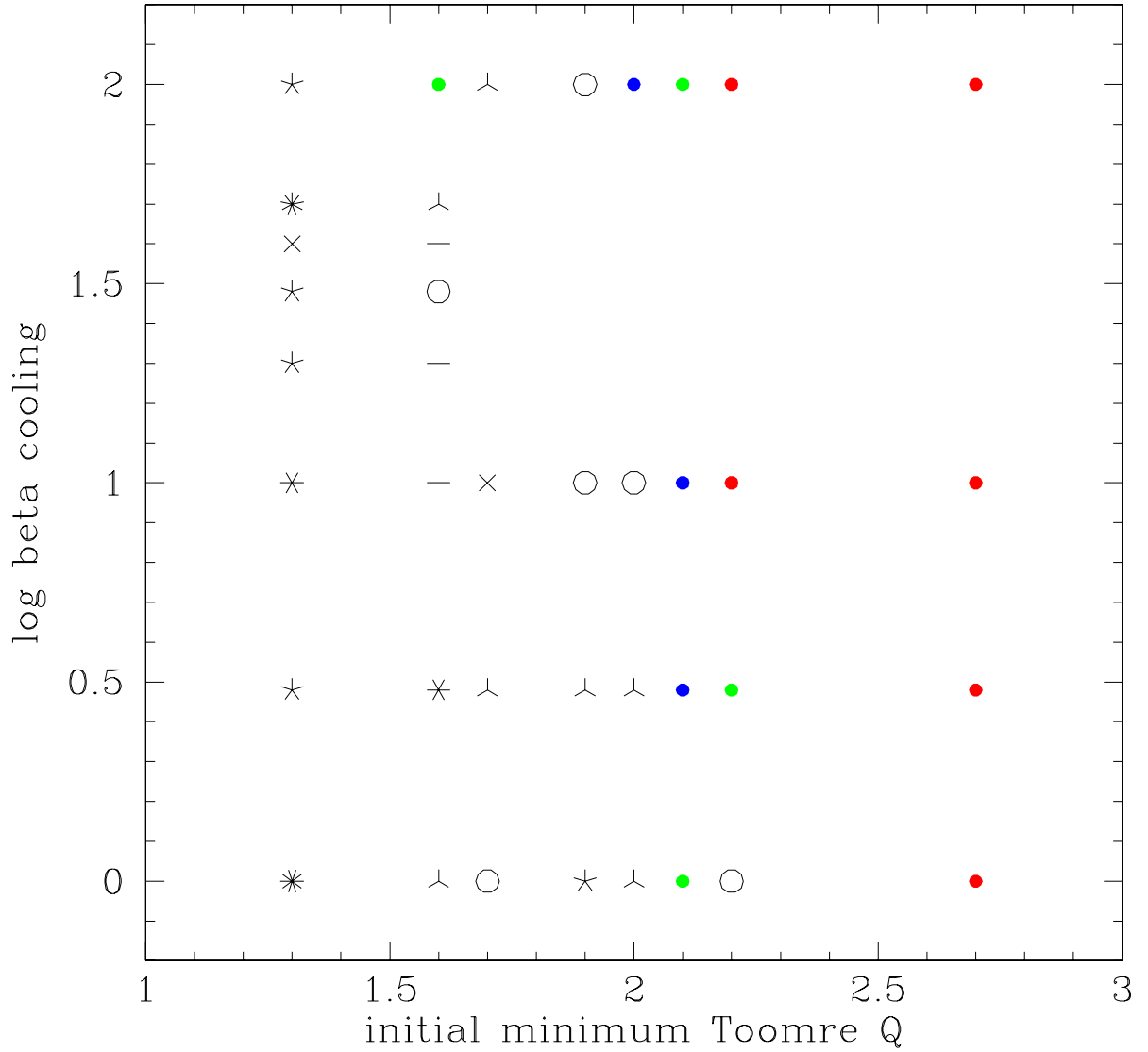


Fig. 4.— Results for the models, plotted as a function of the minimum of the initial Toomre (1964) Q stability parameter and the beta cooling parameter (see Table 1). Symbols denote the degree of growth of nonaxisymmetry or fragmentation, as follows: red = little growth, green = moderate growth, blue = significant growth, black = fragmentation into virtual protoplanets (VPs), with the symbol shape denoting the maximum number of VPs formed (e.g., circles denote single VPs, bars denote two VPs, six pointed-stars denote six VPs, etc.)

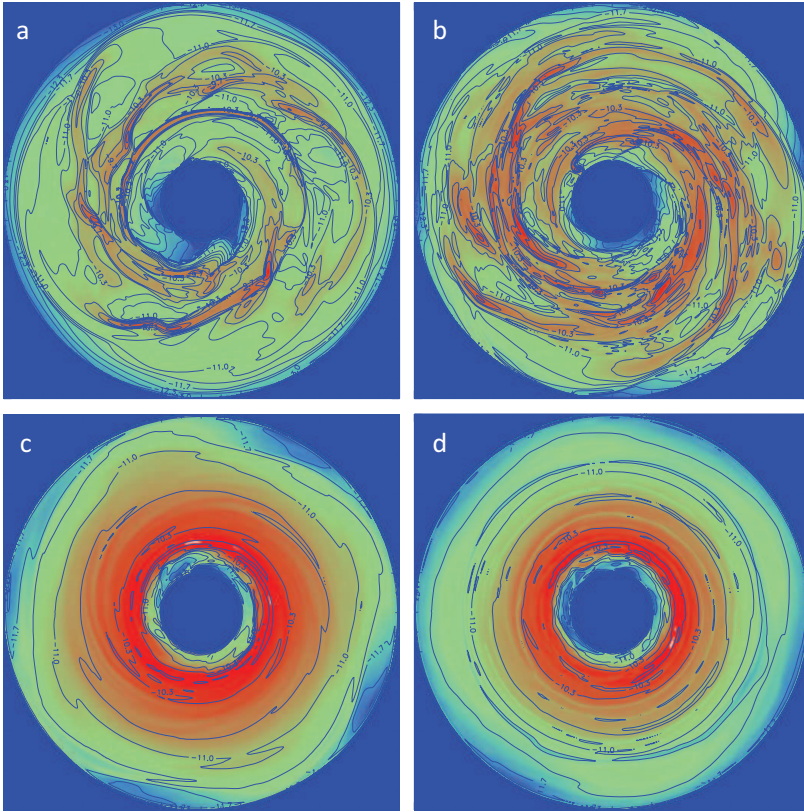


Fig. 5.— Equatorial (midplane) density contours for (a) model 1.3-1 after 244 yr, (b) model 1.3-100 after 342 yr, (c) model 2.7-1 after 450 yr, and (d) model 2.7-100 after 414 yr, plotted as in Figure 3.

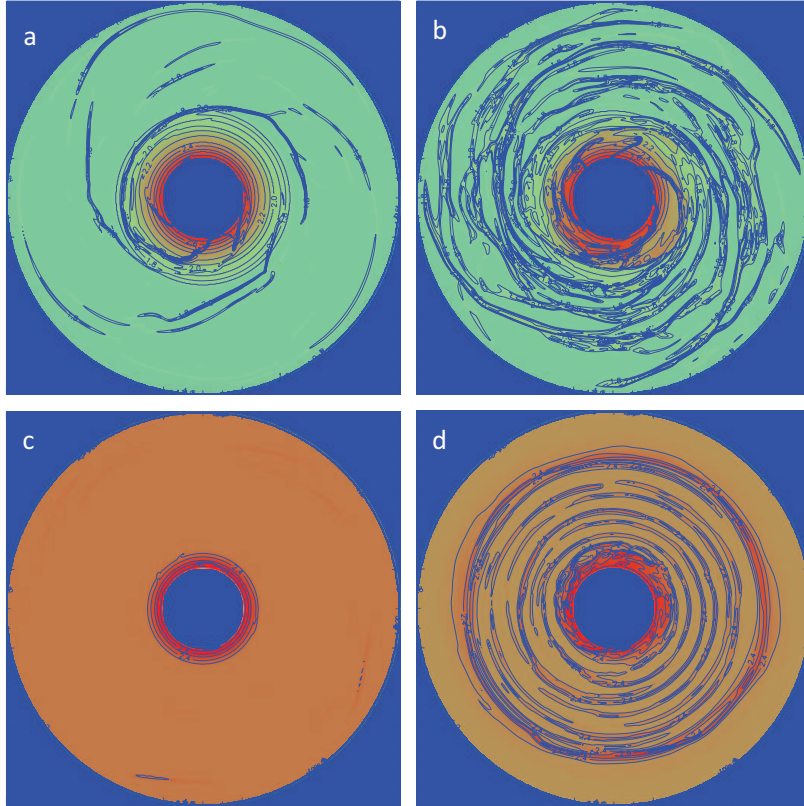


Fig. 6.— Equatorial (midplane) temperature contours for (a) model 1.3-1 after 244 yr, (b) model 1.3-100 after 342 yr, (c) model 2.7-1 after 450 yr, and (d) model 2.7-100 after 414 yr, plotted as in Figure 3. Models 1.3-1 and 1.3-100 have minimum temperatures of 40 K (light green color), while models 2.7-1 and 2.7-100 have minimum temperatures of 180 K (light orange color).

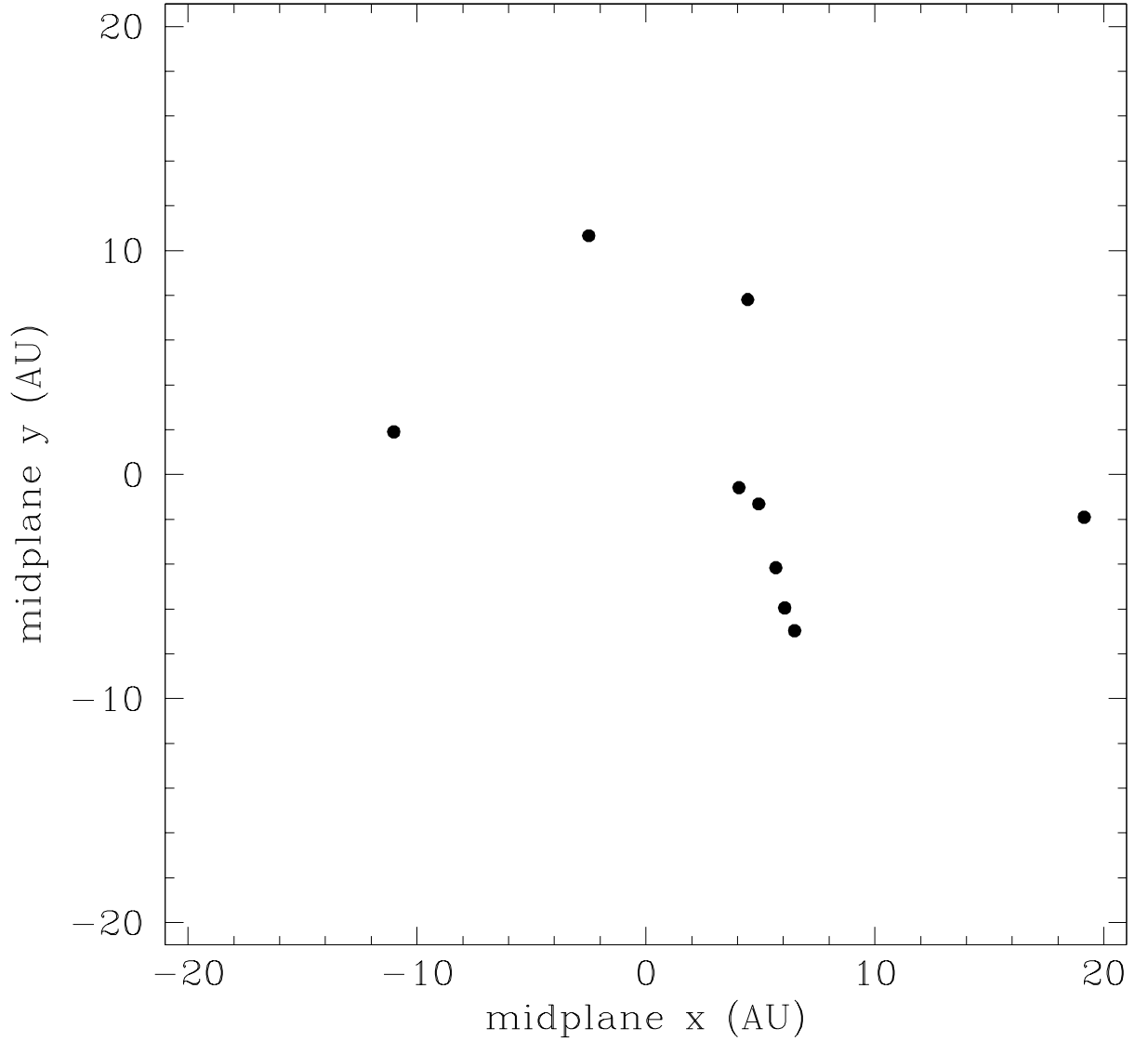


Fig. 7.— Midplane locations of the nine VPs still active in model 1.3-1 at the final time of 244 yr, for comparison to the midplane density and temperature contours shown in Figures 5a and 6a, respectively. The VPs are not associated with any specific spiral arms due to the ensuing chaotic evolution of both their orbits and the gas density maxima since the creation of the VPs.

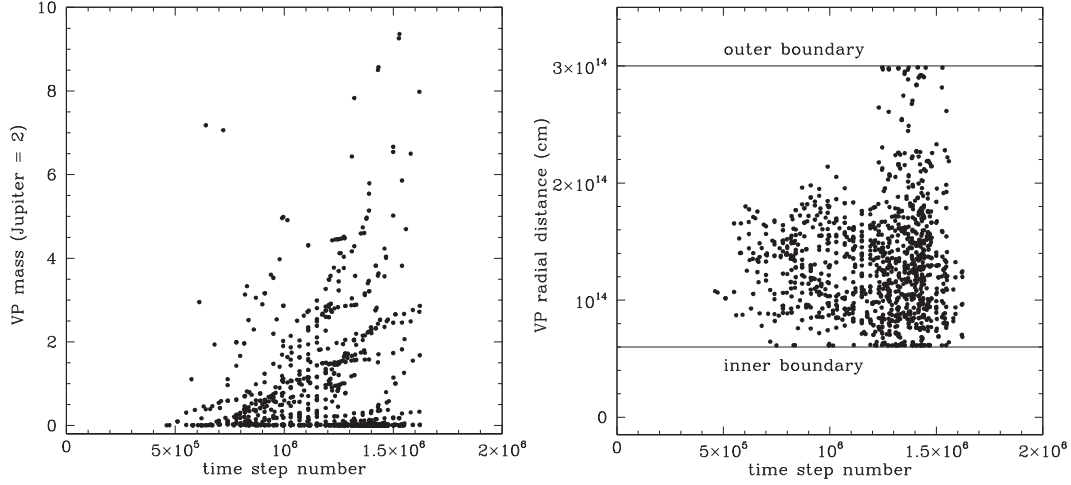


Fig. 8.— Masses (left) and orbital radii (right) as a function of time step number for all of the VPs formed by the eight models starting with initial minimum Toomre $Q = 1.3$, sampled every 40,000 time steps throughout their evolutions. The masses increase by BHL accretion, and the orbital radii both increase and decrease after forming in the about 6 AU to 10 AU region. VPs that hit the inner or outer boundaries are removed from the evolutions.

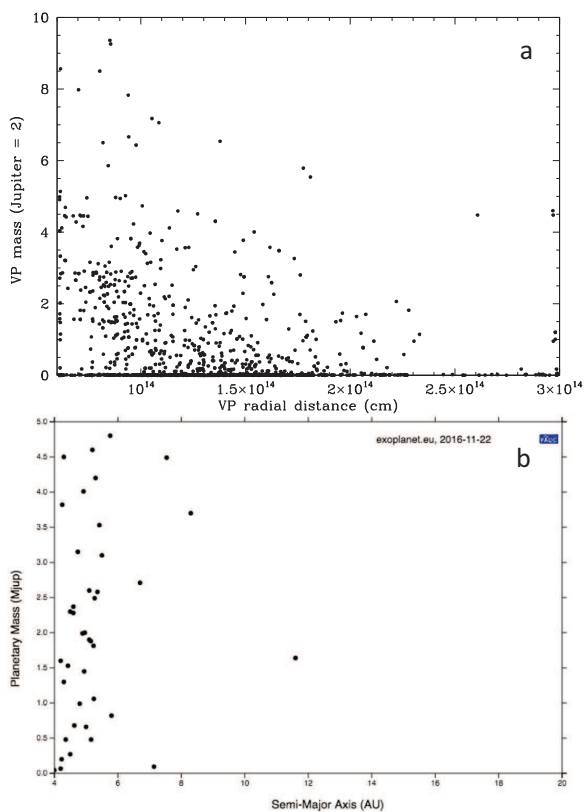


Fig. 9.— A first look at a possible population synthesis model for gas giants formed by disk instability (a) compared to all exoplanets (b) in the Extrasolar Planets Encyclopedia (exoplanets.eu) as of November 22, 2016, for masses between 0 and $5 M_J$ and semi-major axes between 4 AU and 20 AU. The masses and orbital radii of all of the VPs formed by the eight models starting with initial minimum Toomre $Q = 1.3$ are shown in (a), sampled about 40 times throughout their evolutions. While the distributions look similar for semi-major axes less than 6 AU, these models predict that there should be a significant number of gas giants with masses of about $1 M_J$ and semi-major axes of about 6 AU to 16 AU remaining to be discovered.

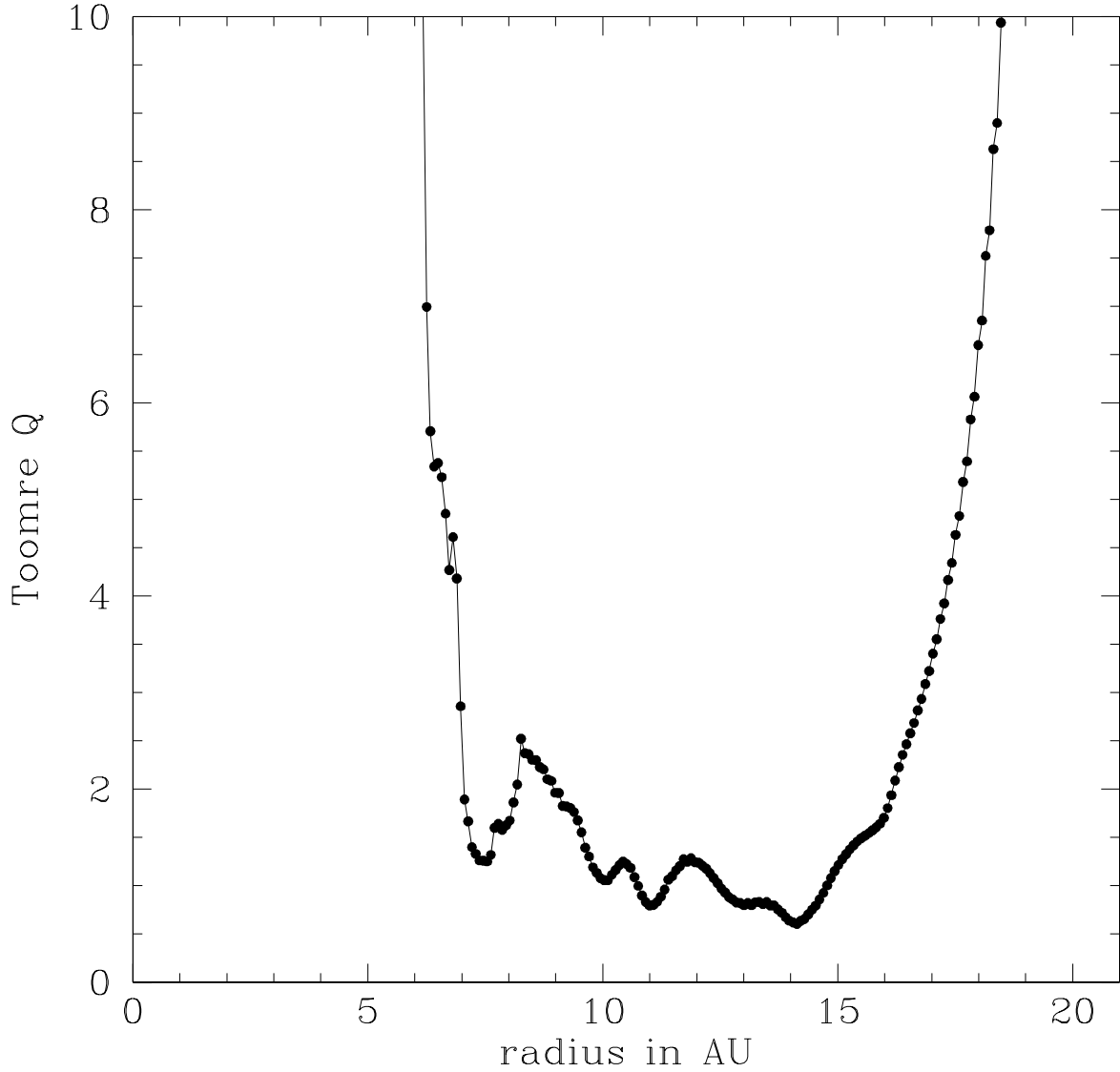


Fig. 10.— Azimuthally averaged radial profile of the Toomre Q parameter for model 1.3-1 at a time of 104 yrs, when the disk non-axisymmetry became so strong that a VP had to be inserted, marking the onset of fragmentation. The minimum Q value at that time is 0.61, consistent with the results of Takahashi et al. (2016).